iScience

CellPress
OPEN ACCESS

Article

Temporal transcriptome features identify early skeletal commitment during human epiphysis development at single-cell resolution

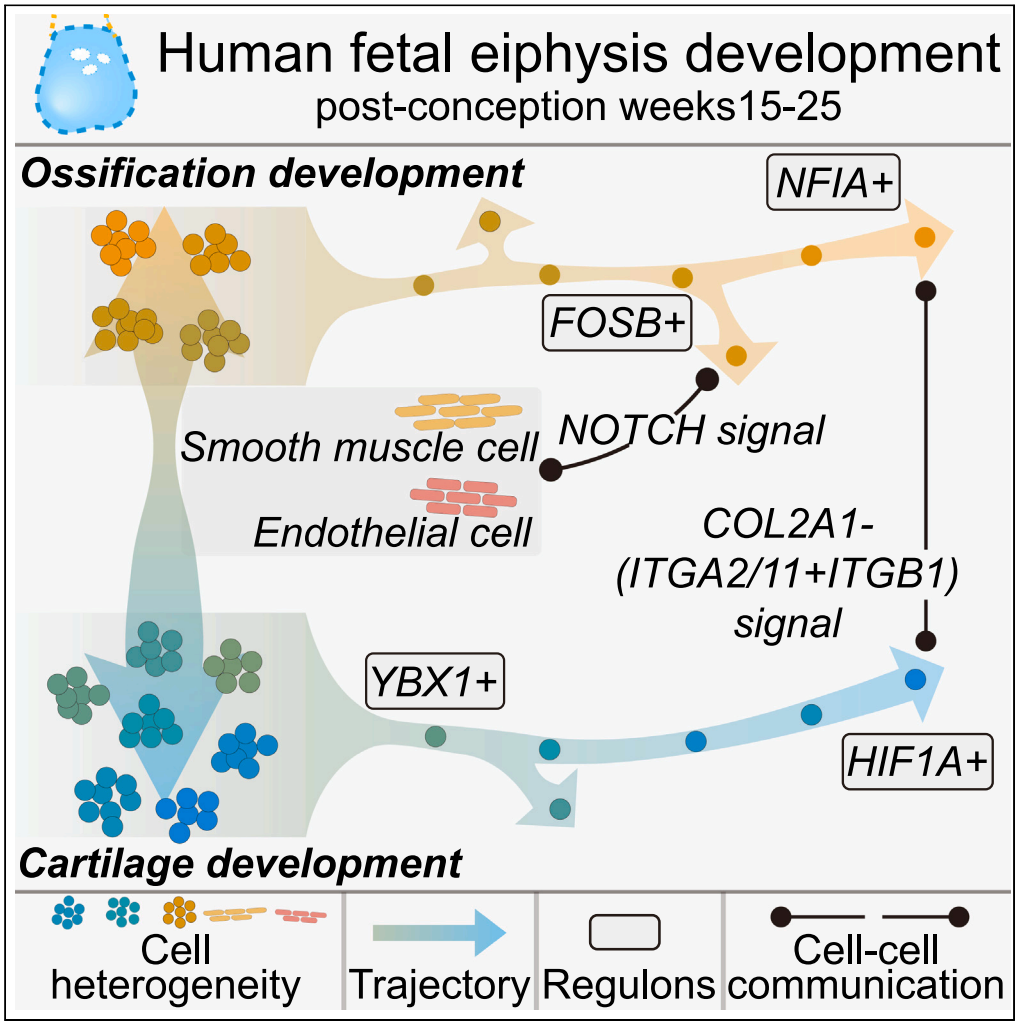

Zhonghao Deng, Shengwei Rong, Lu Gan, ..., Xiaoyong Zheng, Liping Huang, Liang Zhao

lphuang2006@126.com (L.H.)
lzhaonf@126.com (L.Z.)

Highlights

Single-cell analyses identify human fetal epiphysis cell subtypes

Distinct collagen expressions indicate commitment to ossification or cartilage

Transcriptional signals YBX1, HIF1A, FOSB, and NFIA change over cell trajectories

NOTCH signal may involve in cartilage canal formation and ossification development

Deng et al., iScience 26, 107200
August 18, 2023 © 2023
https://doi.org/10.1016/j.isci.2023.107200

iScience

CellPress
OPEN ACCESS

Article

Temporal transcriptome features identify early skeletal commitment during human epiphysis development at single-cell resolution

Zhonghao Deng,[1,2,7] Shengwei Rong,[1,2,7] Lu Gan,[1,2,7] Fuhua Wang,[1,2,7] Liangxiao Bao,[1] Fang Cai,[4] Zheting Liao,[1,2] Yu Jin,[1,2] Shuhao Feng,[1,2] Zihang Feng,[1,2] Yiran Wei,[1,2] Ruge Chen,[1,2] Yangchen Jin,[1,2] Yanli Zhou,[3] Xiaoyong Zheng,[5] Liping Huang,[3,*] and Liang Zhao[1,2,6,8,*]

SUMMARY

Human epiphyseal development has been mainly investigated through radiological and histological approaches, uncovering few details of cellular temporal genetic alternations. Using single-cell RNA sequencing, we investigated the dynamic transcriptome changes during post-conception weeks (PCWs) 15–25 of human distal femoral epiphysis cells. We find epiphyseal cells contain multiple subtypes distinguished by specific markers, gene signatures, Gene Ontology (GO) enrichment analysis, and gene set variation analysis (GSVA). We identify the populations committed to cartilage or ossification at this time, although the secondary ossification centers (SOCs) have not formed. We describe the temporal alternation in transcriptional expression utilizing trajectories, transcriptional regulatory networks, and intercellular communication analyses. Moreover, we find the emergence of the ossification-committed population is correlated with the *COL2A1-(ITGA2/11+ITGB1)* signaling. *NOTCH* signaling may contribute to the formation of cartilage canals and ossification via *NOTCH* signaling. Our findings will advance the understanding of single-cell genetic changes underlying fetal epiphysis development.

INTRODUCTION

The epiphysis is the round-shaped expansion of long bones at both ends, forming joints with adjacent bones. The formation and development of epiphysis are significant to the skeletal development of warm-blooded mammals.[1] Abnormal development of epiphysis may lead to pathological changes characterized by dwarfism and young arthritis, termed epiphyseal dysplasia.[2,3] The human epiphysis forms in the embryonic stage constituted by hyaline cartilage tissue.[4,5] With development, the epiphysis gradually expands and the cartilage canals begin to form inside.[6] Later the secondary ossification center (SOC) occurs due to the vascular invasion from outside.[7–9] The presence time of SOCs varies significantly with the location and species.[10,11] As SOCs develop, ossification tissue replaces cartilage tissue, occupying the central area and separating the growth plate and articular cartilage.[12,13] The epiphysis engages in multiple biological functions, including load-bearing, bone remodeling, metabolism, and immunity.[14,15]

The development of epiphysis lasts from embryo to adolescence, classified into 16 stages in a rabbit study.[16] By means of phase-contrast X-ray computed tomography and magnetic resonance imaging, the distal femoral epiphysis can be recognized 18 days after the conception of human embryos. At post-conception weeks (PCWs) 10–11, cartilage canals appear at both ends of the femoral epiphysis. The cartilage canals are channel-like structures composed of muscular arterioles, venules, loose connective tissue, and perivascular capillaries that form networks inside the epiphysis prior to the appearance of SOCs, contributing to perichondral and endochondral bone formation.[6] Next, SOCs appear in the epiphysis, which marks the initiation of epiphyseal ossification. However, the progress of epiphysis development in humans as well as laboratory animals like mice, rats, and rabbits was observed mainly through radiological and histological technics.[10,14,17,18] The molecular mechanisms that drive the development of epiphysis have not yet been fully elucidated.

Recent advances in single-cell omics technic have enabled a more comprehensive understanding of cellular diversity and temporal trajectories.[19–21] Here, we applied high-throughput single-cell

[1]Department of Orthopaedic Surgery, Nanfang Hospital, Southern Medical University, Guangzhou, Guangdong 510515, China

[2]Guangdong Provincial Key Laboratory of Construction and Detection in Tissue Engineering, Southern Medical University, Guangzhou, Guangdong 510515, China

[3]Department of Obstetrics and Gynecology, Southern Medical University Nanfang Hospital, Guangzhou, Guangdong 510515, China

[4]Department of Obstetrics and Gynecology, Southern Medical University Nanfang Hospital Taihe Branch, Guangzhou, Guangdong 510515, China

[5]Orthopaedic Department, The 8th medical center of Chinese PLA General Hospital, Beijing 100091, China

[6]Department of Orthopaedic Surgery, Shunde First People Hospital, Foshan, Guangdong 528300, China

[7]These authors contributed equally

[8]Lead contact

*Correspondence: lphuang2006@126.com (L.H.), lzhaonf@126.com (L.Z.)

https://doi.org/10.1016/j.isci.2023.107200

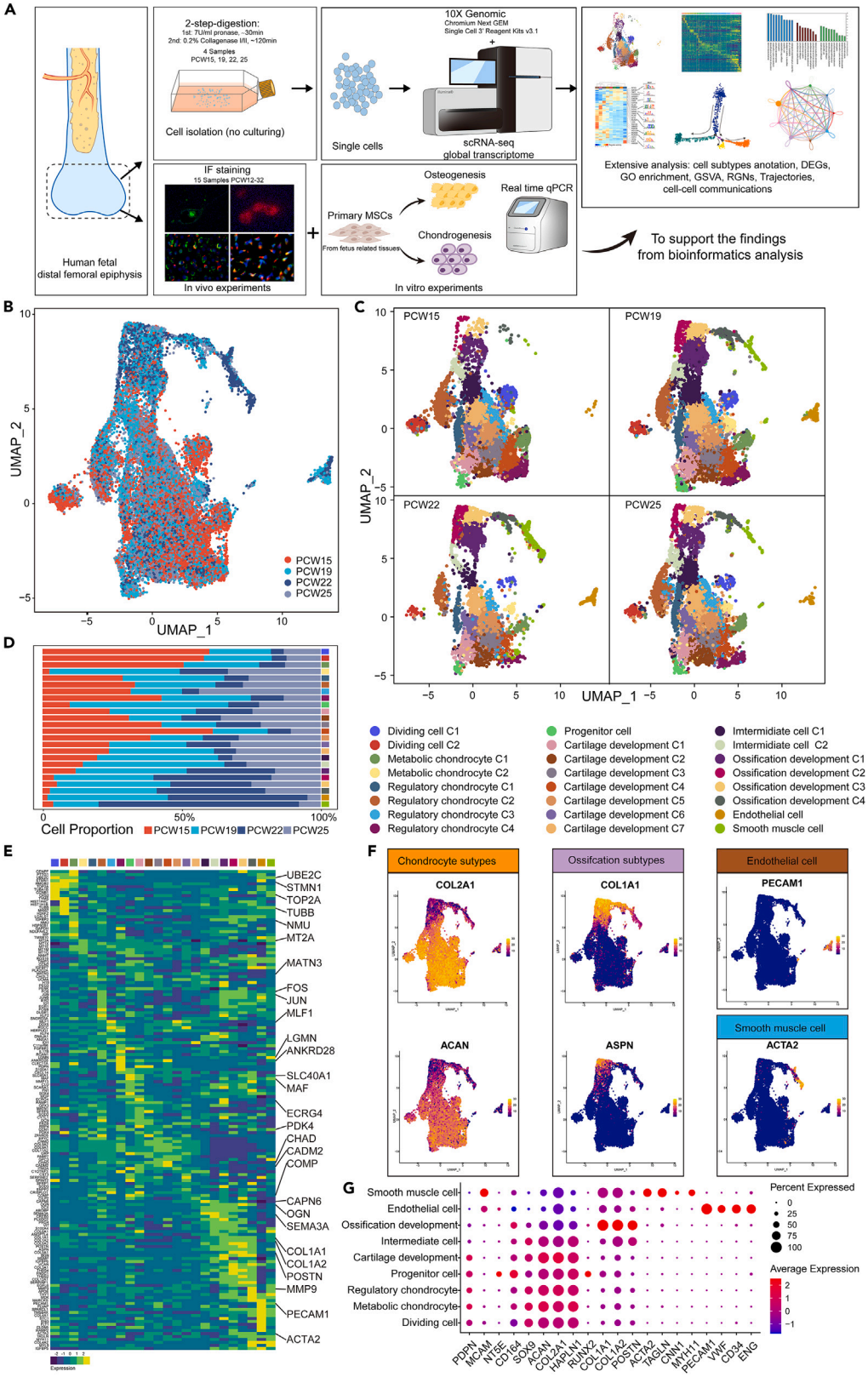
A
Human fetal distal femoral epiphysis
2-step-digestion:
1st: 7U/ml pronase, ~30min
2nd: 0.2% Collagenase I/II, ~120min
4 Samples
PCW15, 19, 22, 25
Cell isolation (no culturing)
IF staining
15 Samples PCW12-32
In vivo experiments
10X Genomic
Chromium Next GEM
Single Cell 3' Reagent Kits v3.1
Single cells
scRNA-seq
global transcriptome
Primary MSCs
From fetus related tissues
Osteogenesis
Chondrogenesis
Real time qPCR
In vitro experiments
Extensive analysis: cell subtypes anotation, DEGs, GO enrichment, GSVA, RGNs, Trajectories, cell-cell communications
To support the findings from bioinformatics analysis
B
UMAP_2
UMAP_1
PCW15
PCW19
PCW22
PCW25
C
PCW15
PCW19
PCW22
PCW25
UMAP_2
UMAP_1
D
Cell Proportion
PCW15 PCW19 PCW22 PCW25
Dividing cell C1
Dividing cell C2
Metabolic chondrocyte C1
Metabolic chondrocyte C2
Regulatory chondrocyte C1
Regulatory chondrocyte C2
Regulatory chondrocyte C3
Regulatory chondrocyte C4
Progenitor cell
Cartilage development C1
Cartilage development C2
Cartilage development C3
Cartilage development C4
Cartilage development C5
Cartilage development C6
Cartilage development C7
Imtermidiate cell C1
Imtermidiate cell C2
Ossification development C1
Ossification development C2
Ossification development C3
Ossification development C4
Endothelial cell
Smooth muscle cell
E
UBE2C
STMN1
TOP2A
TUBB
NMU
MT2A
MATN3
FOS
JUN
MLF1
LGMN
ANKRD28
SLC40A1
MAF
ECRG4
PDK4
CHAD
CADM2
COMP
CAPN6
OGN
SEMA3A
COL1A1
COL1A2
POSTN
MMP9
PECAM1
ACTA2
Expression
F
Chondrocyte sutypes
COL2A1
ACAN
Ossifcation subtypes
COL1A1
ASPN
Endothelial cell
PECAM1
Smooth muscle cell
ACTA2
G
Smooth muscle cell
Endothelial cell
Ossification development
Intermediate cell
Cartilage development
Progenitor cell
Regulatory chondrocyte
Metabolic chondrocyte
Dividing cell
PDPN MCAM NT5E CD164 SOX9 ACAN COL2A1 HAPLN1 RUNX2 COL1A1 COL1A2 POSTN ACTA2 TAGLN CNN1 MYH11 PECAM1 VWF CD34 ENG
Percent Expressed
0
25
50
75
100
Average Expression
2
1
0
−1

Figure 1. Cell subtypes in human fetal epiphysis identified by scRNA-seq

(A) Schematic of performing cell isolation, scRNA-seq, IF, and extensive analysis methods.

(B) UMAP of scRNA-seq epiphyseal cells colored by time points.

(C) UMAPs of scRNA-seq epiphyseal cells colored by unsupervised clustering of each sample.

(D) Cell proportion of each subtype in each sample.

(E) Heatmap of the average expression level of selected cell-subtype-specific markers for each subtype as identified by Wilcoxon rank-sum test of scRNA-seq data. See Figure S1D, Table S1.

(F) UMAPs of scRNA-seq epiphyseal cells colored by *COL2A1*, *ACAN*, *COL1A1*, *ASPN*, *PECAM1*, and *ACTA2*. Cells fell into 14 chondrocyte subtypes, 4 ossification subtypes, 1 endothelial cell subtype, and 1 smooth muscle cell subtype. See Figure S1F.

(G) Canonical lineage marker expression in epiphyseal cells from scRNA-seq data.

transcriptomics sequencing to the human distal femoral epiphysis samples at PCW15–25 and performed the analysis with extensive algorithms to reveal the dynamic changes at the single-cell level. We identified the epiphyseal cell heterogeneity and found that before the emergence of SOCs, some epiphyseal cells might have determined the commitment toward cartilage or ossification by evaluating the pattern of gene expression. We constructed a sequence map of human fetal epiphyseal development, providing a panoramic dataset encompassing cell subtypes, cell trajectories, cell transcription regulatory networks, and intercellular communication. We performed immunohistology fluorescence (IF) staining in vivo and differentiation experiments of osteogenesis and chondrogenesis *in vitro* to support some of the findings from the earlier data analysis. In addition, we found the ossification-committed populations may contribute to the formation of cartilage canals. This study provides a developmental atlas for understanding the cellular biological process of human epiphysis development.

RESULTS

Single-cell RNA sequencing (scRNA-seq) identifies chondrocyte subtypes, endothelial, and smooth muscle cells in fetal epiphysis

In this study, four fetal distal femoral epiphysis samples at PCW15, PCW19, PCW22, and PCW25 were collected, digested, and cell isolated. Next, scRNA-seq was utilized to generate a complementary view of cell diversity at the mRNA level from these samples by using the 10X Genomics platform (see STAR Methods) (Figures 1A and 1B). After quality control (Figures S1A–S1C), 35,686 epiphyseal cells were retained, integrated after batch effects correction, clustered by unsupervised graph-based algorithm, and visualized using Uniform Manifold Approximation and Projection (UMAP) using the R package Seurat[22](version 4.1.1) (see STAR Methods), resulting in 24 subtypes (Figure 1C). All subtypes were detectable in all samples, although their proportions varied at different time points (Figures 1D and S1E). These results suggest that during the development of human fetal epiphysis, various cell groups may have formed in the early stage of development, and the proportion of each cell group may alter subsequently due to division or differentiation.

Marker genes of each subtype were computed to obtain the transcriptomic signatures (Figures 1E and S1D, Table S1). The top 50 markers ordered by the incremental-adjusted p value of each subtype were applied to Gene Ontology (GO) enrichment analysis (Figure S2, Table S1). Canonical marker genes of predicted lineages in the epiphysis, including chondrocyte (*ACAN*, *SOX9*, *COL2A1*, and *HAPLN1*),[23–25] endothelium (*PECAM1*, *VWF*, *CD34*, and *ENG*),[26] and smooth muscle (*ACTA2*, *TAGLN*, *CNN1*, and *MYH11*)[27] were used to verify the identities of each subtype. Collectively, human fetal epiphyseal cells contain sixteen chondrocyte subtypes (highly expressed *ACAN*, *SOX9*, *COL2A1*, and *HAPLN1*), one vascular endothelial cell subtype (highly expressed *PECAM1*, *VWF*, *CD34*, and *ENG*), one pericyte/vascular smooth muscle cell subtype (highly expressed *ACTA2*, *TAGLN*, *CNN1*, and *MYH11*), four subtypes highly expressed *COL1A1*, *COL1A2*, *ASPN*, and *POSTN* (likely ossification lineages),[28] and two subtypes moderately expressed *COL2A1* and *COL1A1* (likely intermediate cell) (Figures 1F and S1F, Table S1). Furthermore, according to the GO biological process (GOBP) results, the sixteen chondrocyte subtypes were classified as two proliferating subtypes (engaged in GOBP: cell division), two metabolism subtypes (engaged in GOBP: multiple metabolic processes), four regulation subtypes (engaged in GOBP: multiple regulatory processes), one progenitor subtype (highly expressed *PDPN*, *NT5E*, and *CD164*; engaged in GOBP: cell differentiation), and seven cartilage development subtypes (engaged in GOBP: cartilage development) (Figures 1G and S2). IF staining of collagen type I (COL1), collagen type II alpha 1 chain (COL2A1), von Willebrand factor (VWF), and α-smooth muscle actin (αSMA, encoded by ACTA2) on sagittal sections showed the locations of lineages mentioned earlier (see STAR Methods). COL1-positive areas were located close to

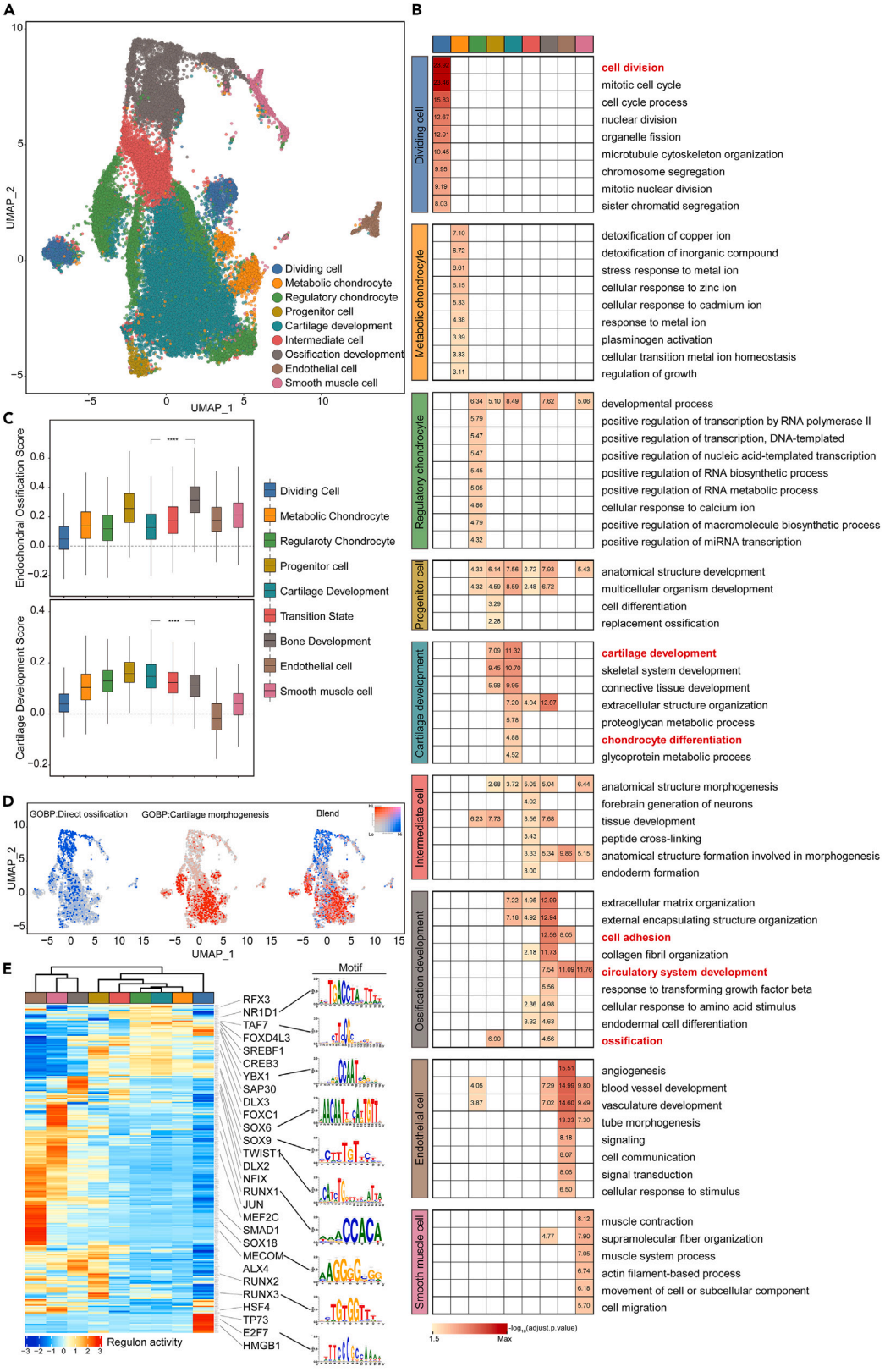
A
UMAP_2
UMAP_1
Dividing cell
Metabolic chondrocyte
Regulatory chondrocyte
Progenitor cell
Cartilage development
Intermediate cell
Ossification development
Endothelial cell
Smooth muscle cell
B
Dividing cell
cell division
mitotic cell cycle
cell cycle process
nuclear division
organelle fission
microtubule cytoskeleton organization
chromosome segregation
mitotic nuclear division
sister chromatid segregation
Metabolic chondrocyte
detoxification of copper ion
detoxification of inorganic compound
stress response to metal ion
cellular response to zinc ion
cellular response to cadmium ion
response to metal ion
plasminogen activation
cellular transition metal ion homeostasis
regulation of growth
Regulatory chondrocyte
developmental process
positive regulation of transcription by RNA polymerase II
positive regulation of transcription, DNA-templated
positive regulation of nucleic acid-templated transcription
positive regulation of RNA biosynthetic process
positive regulation of RNA metabolic process
cellular response to calcium ion
positive regulation of macromolecule biosynthetic process
positive regulation of miRNA transcription
Progenitor cell
anatomical structure development
multicellular organism development
cell differentiation
replacement ossification
Cartilage development
cartilage development
skeletal system development
connective tissue development
extracellular structure organization
proteoglycan metabolic process
chondrocyte differentiation
glycoprotein metabolic process
Intermediate cell
anatomical structure morphogenesis
forebrain generation of neurons
tissue development
peptide cross-linking
anatomical structure formation involved in morphogenesis
endoderm formation
Ossification development
extracellular matrix organization
external encapsulating structure organization
cell adhesion
collagen fibril organization
circulatory system development
response to transforming growth factor beta
cellular response to amino acid stimulus
endodermal cell differentiation
ossification
Endothelial cell
angiogenesis
blood vessel development
vasculature development
tube morphogenesis
signaling
cell communication
signal transduction
cellular response to stimulus
Smooth muscle cell
muscle contraction
supramolecular fiber organization
muscle system process
actin filament-based process
movement of cell or subcellular component
cell migration
-log10(adjust.p.value)
Max
C
Endochondral Ossification Score
Cartilage Development Score
Dividing Cell
Metabolic Chondrocyte
Regularoty Chondrocyte
Progenitor cell
Cartilage Development
Transition State
Bone Development
Endothelial cell
Smooth muscle cell
D
GOBP:Direct ossification
GOBP:Cartilage morphogenesis
Blend
UMAP_2
UMAP_1
E
Motif
RFX3
NR1D1
TAF7
FOXD4L3
SREBF1
CREB3
YBX1
SAP30
DLX3
FOXC1
SOX6
SOX9
TWIST1
DLX2
NFIX
RUNX1
JUN
MEF2C
SMAD1
SOX18
MECOM
ALX4
RUNX2
RUNX3
HSF4
TP73
E2F7
HMGB1
Regulon activity

Figure 2. Cartilage and ossification development populations identified by scRNA-seq

(A) UMAP of scRNA-seq epiphyseal cells colored by manual combined populations.

(B) Heatmap of representative GOBP enriched terms with lowest adjusted p values of each population.

(C) Boxplots of Endochondral ossification-associated and Cartilage development-associated genes expression score of each population (Error bar represent mean ± SD) (t-test)(****$p < 0.0001$). See Tables S3 and S4.

(D) Blended UMAPs of scRNA-seq epiphyseal cells colored by GSVA enrichment scores of GOBP: Direct ossification associated (blue) and GOBP: Cartilage morphogenesis-associated genes (red). See Table S5.

(E) Heatmap of the regulons with differential activity scores in each population and selected motifs for the regulons of particular interest.

cartilage canals. COL2A1 was expressed more widely than COL1 and locally aggregated (Figure S1G). VWF and αSMA were expressed in the inner wall of the cartilage canals (Figure S1H).

Transcriptome signatures distinguish differentiation orientations toward cartilage or ossification before SOCs formation in the human fetal epiphysis

To obtain a more intuitive view of the fetal epiphyseal cells, similar subtypes were manually combined and classified into nine populations (dividing cell, metabolic chondrocyte, regulatory chondrocyte, progenitor cell, cartilage development, intermediate cell, ossification development, endothelial cell, and smooth muscle cell) (Figure 2A). The 50 markers ordered by the incremental-adjusted p value of each subtype were applied to GO enrichment analysis as previously described (Table S2). Consistently, each population was well distinguished as dividing cell population was involved in cell division, cartilage development population in cartilage development and chondrocyte differentiation, metabolic chondrocyte population in metal ion metabolism, and regulatory chondrocyte population in the regulation of transcription (Figure 2B). And the ossification development population was involved in cell adhesion, circulatory system development, and ossification (Figure 2B).

The distinction between cartilage and ossification development populations was estimated from multiple perspectives. In one approach, module scores of gene sets associated with endochondral ossification and cartilage development showed a significant difference between cartilage and ossification development populations. The score of the endochondral ossification gene set in the ossification development population was significantly higher than that in the cartilage development population ($p < 0.0001$). And vice versa, the cartilage development score of the cartilage development population was significantly higher than that of the ossification development population ($p < 0.0001$) (Figure 2C, Tables S3 and S4). To reduce bias from gene selection, a non-parametric, unsupervised method for estimating the variation of gene set enrichment named gene set variation analysis (GSVA) (version 1.42.0) was applied to a random subset of 5,000 cells[29] (see STAR Methods). The results showed that the enriched GOBP entries could also distinguish the cartilage and ossification development populations. For example, according to the GSVA results, the cartilage development subtypes participated in cartilage morphogenesis and chondroblast differentiation, while the ossification development subtypes participated in direct ossification and tooth eruption (Figure S3, Table S5). Moreover, the distribution of direct ossification- and cartilage morphogenesis-associated GSVA enrichment scores could also distinguish the cartilage and ossification development populations (Figure 2D).

To identify transcription signals involved in each population, pySCENIC[30] (version 0.11.2), a tool to infer gene regulatory networks (GRNs) and transcription factor regulon activity using the GRNboost algorithm,[31] was performed on our cells (see STAR Methods). The regulon presents as a gene set including one transcription factor with its potential direct-binding targets.[31] Consistently, the hierarchical clustering based on regulon activities could also distinguish the cartilage and ossification development populations (Figure 2E). Moreover, there are several known lineage regulators among the regulons with differential activity scores in the nine populations, such as *SOX9*, a known transcription regulator regulating chondrocyte differentiation, *SOX6*, *TWIST1*, *RUNX1*, and *RUNX2*. The high transcription activity in the dividing cell population is mainly related to cell cycles, such as *TP73*, *E2F7*, *E2F2*, and *TFDP1* (Figure 2E). Collectively, unsupervised clustering, GO enrichment analysis, general expression distribution and the score of selected gene sets, GSVA, and GRNs analysis suggest that human fetal epiphyseal cells determine the orientations toward cartilage or ossification earlier than the emergence of SOCs.

The cartilage development population shows two trajectories in early fetal epiphyseal development

To obtain a dynamic view of the cartilage development population, 500 cells of this population from each time point were subset randomly and integrated, constructing the developmental trajectories by using the

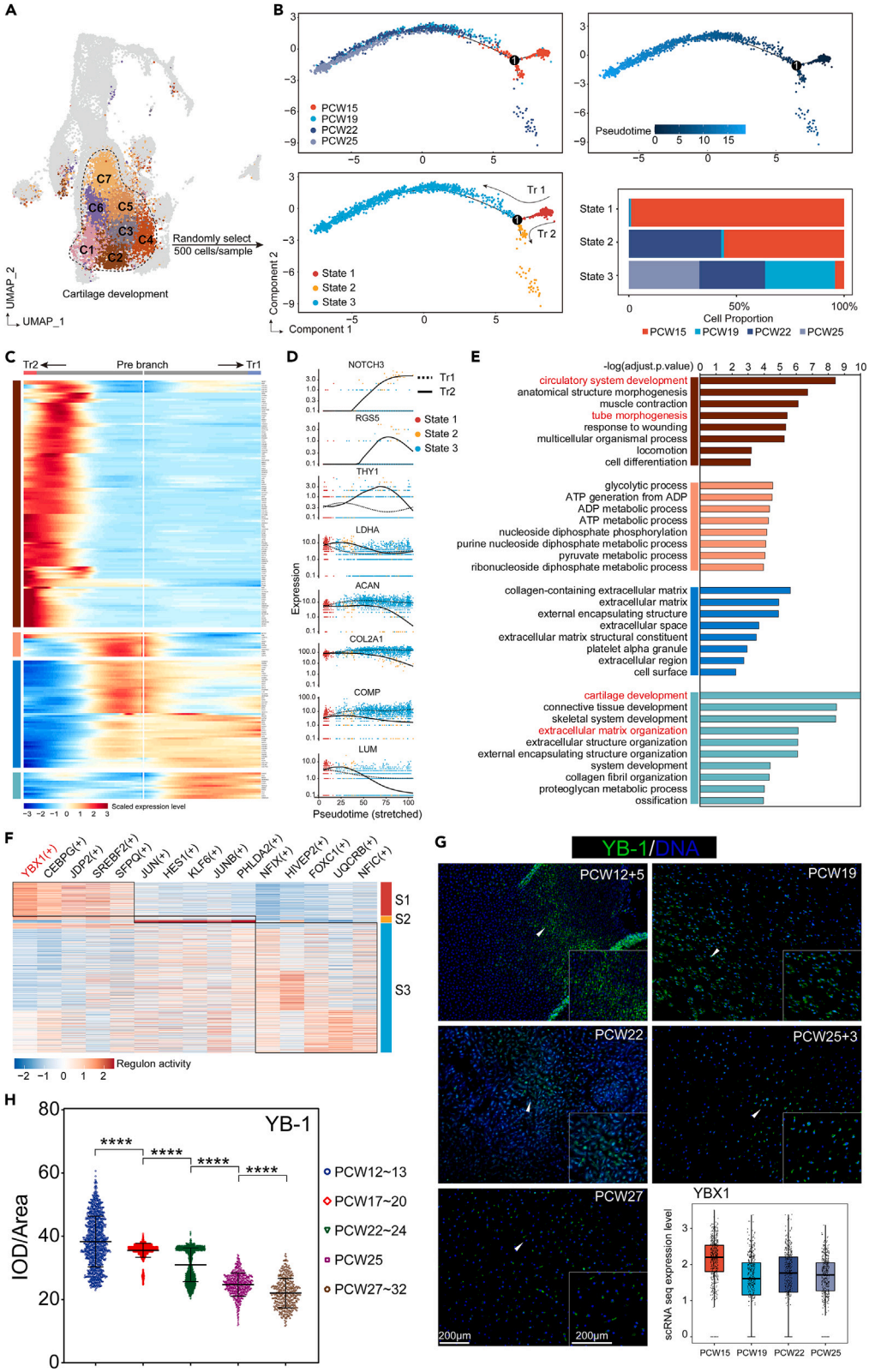
A
C7
C6
C5
C3
C4
C1
C2
Randomly select
500 cells/sample
Cartilage development
UMAP_2
UMAP_1
B
PCW15
PCW19
PCW22
PCW25
Pseudotime
Tr 1
Tr 2
State 1
State 2
State 3
Component 2
Component 1
Cell Proportion
C
Tr2
Pre branch
Tr1
Scaled expression level
D
NOTCH3
RGS5
THY1
LDHA
ACAN
COL2A1
COMP
LUM
Expression
Pseudotime (stretched)
E
-log(adjust.p.value)
circulatory system development
anatomical structure morphogenesis
muscle contraction
tube morphogenesis
response to wounding
multicellular organismal process
locomotion
cell differentiation
glycolytic process
ATP generation from ADP
ADP metabolic process
ATP metabolic process
nucleoside diphosphate phosphorylation
purine nucleoside diphosphate metabolic process
pyruvate metabolic process
ribonucleoside diphosphate metabolic process
collagen-containing extracellular matrix
extracellular matrix
external encapsulating structure
extracellular space
extracellular matrix structural constituent
platelet alpha granule
extracellular region
cell surface
cartilage development
connective tissue development
skeletal system development
extracellular matrix organization
extracellular structure organization
external encapsulating structure organization
system development
collagen fibril organization
proteoglycan metabolic process
ossification
F
YBX1(+)
CEBPG(+)
JDP2(+)
SREBF2(+)
SFPQ(+)
JUN(+)
HES1(+)
KLF6(+)
JUNB(+)
PHLDA2(+)
NFIX(+)
HIVEP2(+)
FOXC1(+)
UQCRB(+)
NFIC(+)
S1
S2
S3
Regulon activity
G
YB-1/DNA
PCW12+5
PCW19
PCW22
PCW25+3
PCW27
200μm
YBX1
scRNA seq expression level
PCW15
PCW19
PCW22
PCW25
H
YB-1
IOD/Area
****
PCW12~13
PCW17~20
PCW22~24
PCW25
PCW27~32

Figure 3. Trajectories of the Cartilage development population and GRNs analysis over the progress

(A) Schematic of approach subsampling cells for trajectory analysis.

(B) Trajectory plots color by samples (top left), pseudotime (top right), and cell states (bottom left). Cell proportion of each state of each sample (bottom right).

(C) Expressions of the top 200 branch-dependent genes with q value < 0.0001. Genes were classified into four clusters.

(D) Selected genes (*NOTCH3*, *RGS5*, *THY1*, *LDHA*, *ACAN*, *COL2A1*, *COMP*, and *LUM*) expression of two trajectories over pseudotime, with dots colored by states.

(E) GO enrichment analysis of clustered genes from (C).

(F) Heatmap of the regulons with differential activity scores in each state.

(G) Represent IF staining of YB-1 (green) on sagittal epiphyseal sections. Boxplot of scRNA-seq epiphyseal cells colored by *YBX1* (Error bar represent mean ± SD). See Figures S4A and S5.

(H) Quantification of YB-1-positive staining by calculating integrated optical density (IOD)/Area of each group (PCW12∼13,n = 2; PCW17∼20, n = 3; PCW22∼24, n = 3; PCW25, n = 3; PCW27∼32, n = 3) (Error bar represent mean ± SD) (test by one-way ANOVA) (****p < 0.0001).

algorithms based on unsupervised feature selection from dense cell clusters and discriminative dimensionality reduction via learning a tree (DDRTree) built in Monocle package (version 2.22.0)[32,33](see STAR Methods) (Figure 3A). The pseudotime used in Monocle is an abstract unit describing the position of cells widely distributed in terms of progress based on the amount of transcriptional change. Within our data, the pseudotime from 0 to 20 reflected the actual developmental time of the samples from PCW15 to PCW25 (Figure 3B). At the start of the trajectory, cells in state 1 were constituted mainly by the sample at PCW15. As development progressed, cells in state 1 passed through a branching point, dividing into trajectory 1 reaching state 3 and trajectory 2 reaching state 2, respectively. The number of cells in state 2 was far less than that in state 3, which suggested that the main trajectory of cartilage development population might start from state 1 to state 3. (Figure 3B).

The top 200 branch-dependent genes with q value < 0.0001 were used to construct the heatmap, showing four distinct expression dynamics gene sets along branch 1 (Figure 3C). The expressions of *NOTCH3*, *RGS5*, and *THY1* in trajectory 2 were higher than those in trajectory 1, while the expressions of *ACAN*, *COL2A1*, and *COMP* were higher in trajectory 1 (Figure 3D). GO enrichment analysis showed that genes with increasing expression levels along with trajectory 1 were involved in cartilage development and extracellular matrix organization, while the genes with increased expression levels along with trajectory 2 were involved in circulatory system development and tube morphogenesis (Figure 3E). This result also suggested that the cells in state 3 might play a major role in the development of epiphyseal cartilage.

Next, the differential regulons activities underlying the cells in each state were calculated by using the FindAllMarker algorithm in Seurat (see STAR Methods). The top 5 regulons with significant high activity in each state were elected to construct a heatmap (Figure 3F). Among the cells in state 1, *YBX1*, a known transcript factor implicated in the regulation of transcription and translation, was of high activity. Since the regulon activity is calculated based on multiple genes regulated by one transcription factor, a high regulon activity is unequal to a high expression of a transcript factor. Thus, the combination of gene expression and regulon activity may help to screen out some significant transcription factors. Through this approach, six transcription factors with detectable expression trends during development were screened out (Figure S4A). The immunofluorescent staining of YB-1 and HIF1A estimated the consistency of this approach. YB-1 showed the highest expressed levels at PCW15 and decreased during development (Figures 3G and 3H). Cells that expressed HIF1A were located close to the cartilage canals. And their expression levels had a similar trend to the gene expression levels detected by scRNA-seq during development (Figures S4B and S4C).

To show the co-localization relationship between transcription factors and their targets and their expression changes over development, we selected three proteins from downstream targets of *HIF1A* or *YBX1* for IF co-staining. *ERRFI1* is a target gene of *HIF1A*, encoding MIG-6 (Figure S4F). IF results showed that both HIF1A and MIG-6 were expressed around the cartilage canal (Figure S4D), and the quantitative dynamic of MIG-6 expression over development was the same as that of HIF1A (Figure S4E). Both *CALR* (encoding CALR) and *CD63* (encoding CD63) are target genes of *YBX1*. The expression of CALR and CD63 tended to decrease gradually from PCW12 to PCW25 according to IF co-staining, exhibiting a similar trend as gene expression (Figures S5A–S5D and S5H). However, compared with PCW25, the expression of CALR and CD63 in PCW27 ∼ 32 samples increased significantly (Figures S5A–S5D).

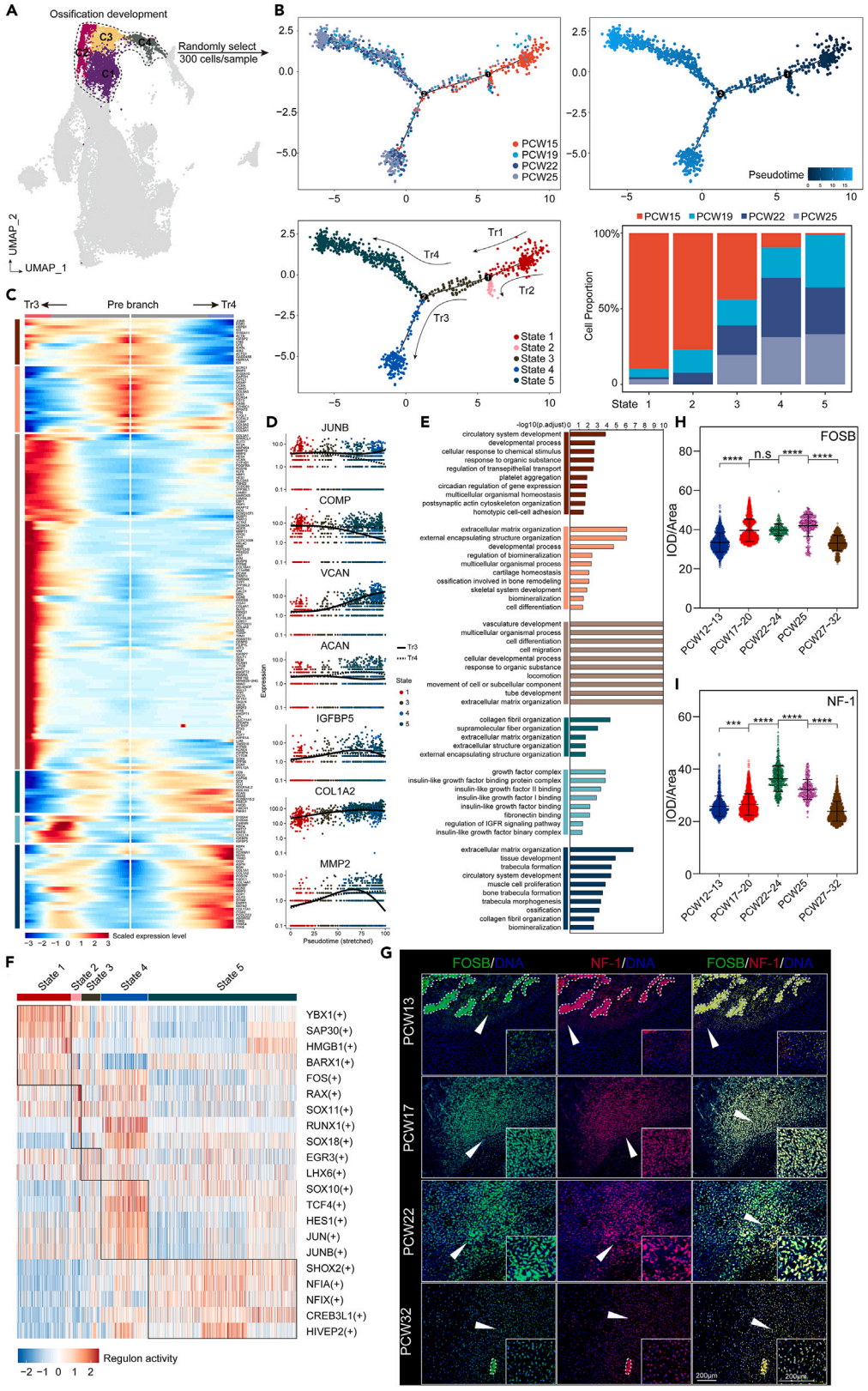
A
Ossification development
C3
C2
C4
C1
Randomly select
300 cells/sample
UMAP_2
UMAP_1
B
PCW15
PCW19
PCW22
PCW25
Pseudotime
Tr1
Tr2
Tr3
Tr4
State 1
State 2
State 3
State 4
State 5
Cell Proportion
100%
50%
0
State 1 2 3 4 5
C
Tr3
Pre branch
Tr4
Scaled expression level
D
JUNB
COMP
VCAN
ACAN
IGFBP5
COL1A2
MMP2
Expression
Pseudotime (stretched)
E
-log10(p.adjust)
circulatory system development
developmental process
cellular response to chemical stimulus
response to organic substance
regulation of transepithelial transport
platelet aggregation
circadian regulation of gene expression
multicellular organismal homeostasis
postsynaptic actin cytoskeleton organization
homotypic cell-cell adhesion
extracellular matrix organization
external encapsulating structure organization
developmental process
regulation of biomineralization
multicellular organismal process
cartilage homeostasis
ossification involved in bone remodeling
skeletal system development
biomineralization
cell differentiation
vasculature development
multicellular organismal process
cell differentiation
cell migration
cellular developmental process
response to organic substance
locomotion
movement of cell or subcellular component
tube development
extracellular matrix organization
collagen fibril organization
supramolecular fiber organization
extracellular matrix organization
extracellular structure organization
external encapsulating structure organization
growth factor complex
insulin-like growth factor binding protein complex
insulin-like growth factor II binding
insulin-like growth factor I binding
insulin-like growth factor binding
fibronectin binding
regulation of IGFR signaling pathway
insulin-like growth factor binary complex
extracellular matrix organization
tissue development
trabecula formation
circulatory system development
muscle cell proliferation
bone trabecula formation
trabecula morphogenesis
ossification
collagen fibril organization
biomineralization
Tr3
Tr4
State
H
FOSB
IOD/Area
n.s
PCW12~13
PCW17~20
PCW22~24
PCW25
PCW27~32
I
NF-1
F
State 1
State 2
State 3
State 4
State 5
YBX1(+)
SAP30(+)
HMGB1(+)
BARX1(+)
FOS(+)
RAX(+)
SOX11(+)
RUNX1(+)
SOX18(+)
EGR3(+)
LHX6(+)
SOX10(+)
TCF4(+)
HES1(+)
JUN(+)
JUNB(+)
SHOX2(+)
NFIA(+)
NFIX(+)
CREB3L1(+)
HIVEP2(+)
Regulon activity
G
FOSB/DNA
NF-1/DNA
FOSB/NF-1/DNA
PCW13
PCW17
PCW22
PCW32
200μm

Figure 4. Trajectories of the Ossification development population and GRNs analysis over the progress

(A) Schematic of approach subsampling cells for trajectory analysis.

(B) Trajectory plots color by samples (top left), pseudotime (top right), and cell states (bottom left). Cell proportion of each state of each sample (bottom right).

(C) Expressions of the top 200 branch-dependent genes of branch 2 with q value < 0.0001. Genes were classified into six clusters.

(D) Selected genes (*JUNB*, *COMP*, *VCAN*, *ACAN*, *IGFBP5*, *COL1A2*, and *MMP2*) expression of trajectory 3 and 4 over pseudotime, with dots colored by states.

(E) GO enrichment analysis of clustered genes from (C).

(F) Heatmap of the regulons with differential activity scores in each state.

(G) Represent IF staining of FOSB (green) and NF-1 (red) on sagittal epiphyseal sections. Within the dotted line represents the cartilage canal structure. See Figures S6D, S7, and S8.

(H) Quantification of FOSB-positive staining by calculating IOD/Area of each group (PCW12∼13,n = 2; PCW17∼20, n = 3; PCW22∼24, n = 3; PCW25, n = 3; PCW27∼32, n = 3) (Error bar represent mean ± SD) (test by one-way ANOVA) (n.s, $p \geq 0.05$; ****$p < 0.0001$).

(I) Quantification of NF-1-positive staining by calculating IOD/Area of each group (PCW12∼13,n = 2; PCW17∼20, n = 3; PCW22∼24, n = 3; PCW25, n = 3; PCW27∼32, n = 3) (Error bar represent mean ± SD) (test by one-way ANOVA) (****$p < 0.0001$).

Moreover, human umbilical cord blood mesenchymal stem cells (UBMSCs) were purchased and expanded for chondrogenic differentiation under micromass culture (see STAR Methods) (Figures S5E and S5F). We selected the downstream target genes of YBX1 to analyze the expression level over chondrogenic differentiation. Compared with the expression dynamics of the corresponding gene over cartilage development obtained by single-cell sequencing, the trend of *in vitro* differentiation experiment is similar (Figures S5G and S5H).

The ossification development population shows four trajectories and two branches in early fetal epiphyseal development

Discovering the ossification development population in epiphysis before SOCs formation was unexpected. Similar approaches were also performed on this population to obtain a clear view of its developmental trajectories. A total of 1,200 cells integrated by 300 from each sample randomly constructed the trajectories (Figures 4A and 4B). The pseudotime calculated by Monocle matched the actual developmental time of the samples (Figure 4B). In this progress, the ossification development populations went through two branches, resulting in four trajectories and five states (Figure 4B). The proportion of cells from PCW15 was highest in state 1 and dropped gradually over time. On the contrary, the percentage of cells from other time points gradually increased with time (Figure 4B). Most cells from state 1 transitioned into state 3 through the first branch, resulting in the minimum proportion of state 2. Next, cells from state 3 transitioned into state 4 and state 5 through the second branch (Figure 4B).

The top 100 branch-dependent genes of branch 1 with q value < 0.0001 were used to construct the heatmap, showing three distinct expression dynamics gene sets along branch 1 (Figure S6A). Before reaching the second branch, the expressions of *ACTG1* and *THY1* in trajectory 1 were higher than those in trajectory 2, while *SPARC* and *THBS2* were higher in trajectory 2. The genes correlated with chondrocyte differentiation as *CHI3L1* and *MSMP* showed decreasing expression over time in both trajectories (Figure S6B). GO enrichment analysis of the aforementioned gene sets revealed that genes in trajectory 2 are involved in cell migration and tube development. And cells in trajectory 1 might implicate extracellular matrix organization and ossification (Figure S6C).

Since most cells went through the second branch, trajectory 3 and trajectory 4 might potentially be the main progress during ossification development in this period. Similarly, the top 100 branch-dependent genes of branch 1 with q value < 0.0001 were used to construct the heatmap, showing six distinct expression dynamics gene sets along branch 1 (Figure 4C). After the cells passed through the second branch, the expressions of *JUNB* and *VCAN* in trajectory 3 were higher than those in trajectory 4, while *ACAN*, *COL1A2*, and *MMP2* were higher in trajectory 2 (Figure 4D). Using the aforementioned six gene sets as input, GO enrichment analysis revealed that genes highly expressed in trajectory 3 are involved in vasculature development, cell differentiation, and cell migration. And cells in trajectory 4 might implicate extracellular matrix organization, trabecula formation, and ossification (Figure 4E).

Next, similar approaches determined the differential active regulons in each state. Cells in state 5, with the highest proportion, exhibited high activity of some previously reported transcription signals correlating to

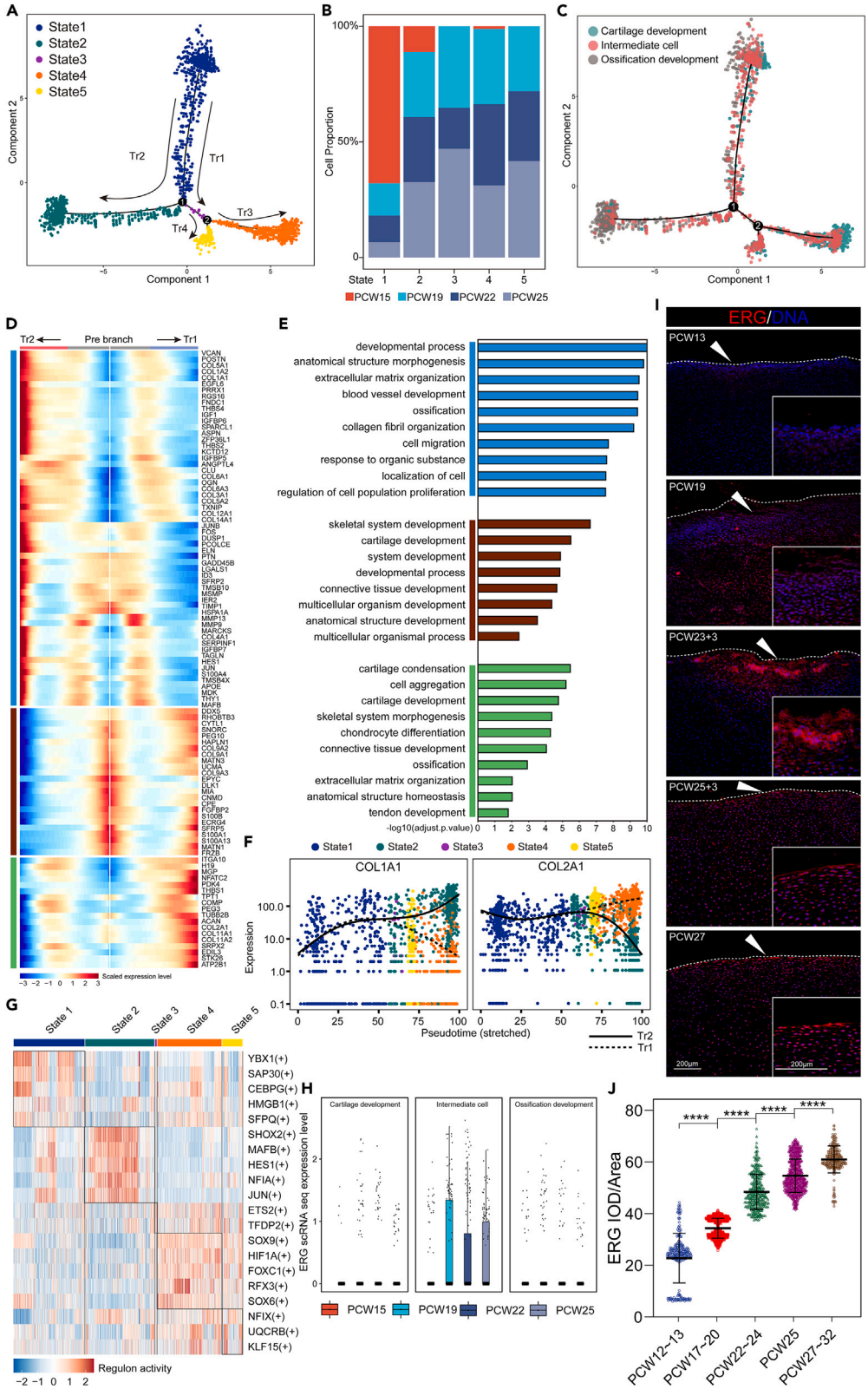
A
State1
State2
State3
State4
State5
Component 2
Component 1
Tr1
Tr2
Tr3
Tr4
B
Cell Proportion
100%
50%
0
State 1 2 3 4 5
PCW15 PCW19 PCW22 PCW25
C
Cartilage development
Intermediate cell
Ossification development
Component 2
Component 1
D
Tr2
Pre branch
Tr1
Scaled expression level
E
developmental process
anatomical structure morphogenesis
extracellular matrix organization
blood vessel development
ossification
collagen fibril organization
cell migration
response to organic substance
localization of cell
regulation of cell population proliferation
skeletal system development
cartilage development
system development
developmental process
connective tissue development
multicellular organism development
anatomical structure development
multicellular organismal process
cartilage condensation
cell aggregation
cartilage development
skeletal system morphogenesis
chondrocyte differentiation
connective tissue development
ossification
extracellular matrix organization
anatomical structure homeostasis
tendon development
-log10(adjust.p.value)
F
State1 State2 State3 State4 State5
COL1A1
COL2A1
Expression
Pseudotime (stretched)
Tr2
Tr1
G
State 1 State 2 State 3 State 4 State 5
YBX1(+)
SAP30(+)
CEBPG(+)
HMGB1(+)
SFPQ(+)
SHOX2(+)
MAFB(+)
HES1(+)
NFIA(+)
JUN(+)
ETS2(+)
TFDP2(+)
SOX9(+)
HIF1A(+)
FOXC1(+)
RFX3(+)
SOX6(+)
NFIX(+)
UQCRB(+)
KLF15(+)
Regulon activity
H
Cartilage development
Intermediate cell
Ossification development
ERG scRNA seq expression level
PCW15 PCW19 PCW22 PCW25
I
ERG/DNA
PCW13
PCW19
PCW23+3
PCW25+3
PCW27
200μm
J
ERG IOD/Area
****
PCW12~13
PCW17~20
PCW22~24
PCW25
PCW27~32

Figure 5. Trajectory and GRNs analysis of integrated cells from the Intermediate, Cartilage development, and Ossification development populations and the transcriptome identified to be expressed in Intermediate cell population

(A) Trajectory plots color by cell states. See Figures S9A and S9B.
(B) Cell proportion of each state of each sample. See Figure S9C.
(C) Trajectory plots color by populations.
(D) Expressions of the top 100 branch-dependent genes of branch 1 with q value < 0.01. Genes were classified into three clusters.
(E) GO enrichment analysis of clustered genes from (D).
(F) *COL1A1* and *COL2A1* expressions of trajectory 1 and 2 over pseudotime, with dots colored by states. See Figure S9D.
(G) *Heatmap of* the regulons with differential activity scores in each state.
(H) Boxplot of transcriptome factor *ERG* exhibited expression specifically in the Intermediate cell population (Error bar represent mean ± SD).
(I) Represent IF staining of ERG (red) on sagittal epiphyseal sections. The dotted line position refers to the distal edge of epiphysis. See Figure S10.
(J) Quantification of ERG-positive staining by calculating IOD/Area of each group (PCW12∼13,n = 2; PCW17∼20, n = 3; PCW22∼24, n = 3; PCW25, n = 3; PCW27∼32, n = 3) (Error bar represent mean ± SD) (test by one-way ANOVA) (****p < 0.0001).

ossification as *SHOX2*, *NFIA*, and *NFIX*[34–36] (Figure 4F). Through the screening of regulon activity and gene expression level, six transcription factors that can be detected and show the trend of time change were obtained (Figure S6D). The immunofluorescent staining of FOSB and NF-1 reflected a consistent trend between the protein and mRNA expression over epiphyseal development (Figures 4G and S6D). The expression of FOSB increased from PCW12 and peaked at PCW25 (Figure 4H), while the protein level of NF-1 peaked at PCW22–24, showing a similar pattern to its mRNA expression (Figures 4I and S6D).

Both *LRP1* and *ATF4* are downstream target genes of *FOSB*. IF results showed that FOSB and LRP1 were co-stained (Figure S7A), and LRP1 expression gradually increased over development (Figure S7C). ATF4 and FOSB were also co-localized (Figure S7B), and the expression of ATF4 increased slightly over development (Figure S7D). We found that the dynamic expression of *LRP1* and *ATF4* in the ossification development population was similar to that of *FOSB* over development (Figures S6D, S7E, and S7F). We obtained human UBMSCs and human placental mesenchymal stem cells (PMSCs) for osteoblastic differentiation *in vitro* (see STAR Methods). We observed that the expression of *LRP1* increased significantly in the early stage of osteoblastic differentiation (Figures S7G and S7H). Moreover, we found that the expression of downstream target genes of FOSB (*FN1*, *KLF6*, *MAPRE2*, *COL3A1*, and *LIMA1*) over osteogenic differentiation was similar to that of scRNA-seq data (Figures S8A–S8C). We also observed the co-location of NF-1 with its two downstream targets (IGF-1 and ASPN) (Figures S8D and S8E). The dynamic expression of IGF-1 and ASPN protein was consistent with the gene expression observed from scRNA-seq (Figures S8F and S8G).

The intermediate cell population distributes evenly during cartilage and ossification development

There was a population of cells expressing a moderate level of *COL2 (COL2A1* and *COL2A2)* and *COL1 (COL1A1* and *COL1A2)* in our data, named intermediate cell. The position of cells in UMAP can partially reflect the cell relationship between one another by the distance.[37] The intermediate cell population was distributed between the cartilage development population and ossification development population in UMAP, indicating similar mRNA features to the two adjacent populations (Figure 2A). GO enrichment analysis revealed that the intermediate cell population might implicate the GOBPs as tissue development, endoderm formation, and extracellular structure organization (Figure 2B). The earlier findings may lead to the inference that the intermediate cell population is a transitional population involved in cartilage and ossification development.

To investigate the dynamic relations among the three populations mentioned earlier, a total of 2,160 cells integrated by 180 from each population from each sample randomly constructed the trajectories (Figure 5A). The pseudotime calculated by Monocle matched the actual developmental time of the samples, and the cells in state 1 mainly came from PCW15 (Figures 5B, S9A, and S9B). The first branch distinctly separated the fate of cells toward cartilage or ossification development but not the cells in the intermediate cell population with a more even distribution in each state (Figure 5C). However, cells from these three populations constitute the cells in state 1, making it difficult to determine which is the "progenitor" of cells in

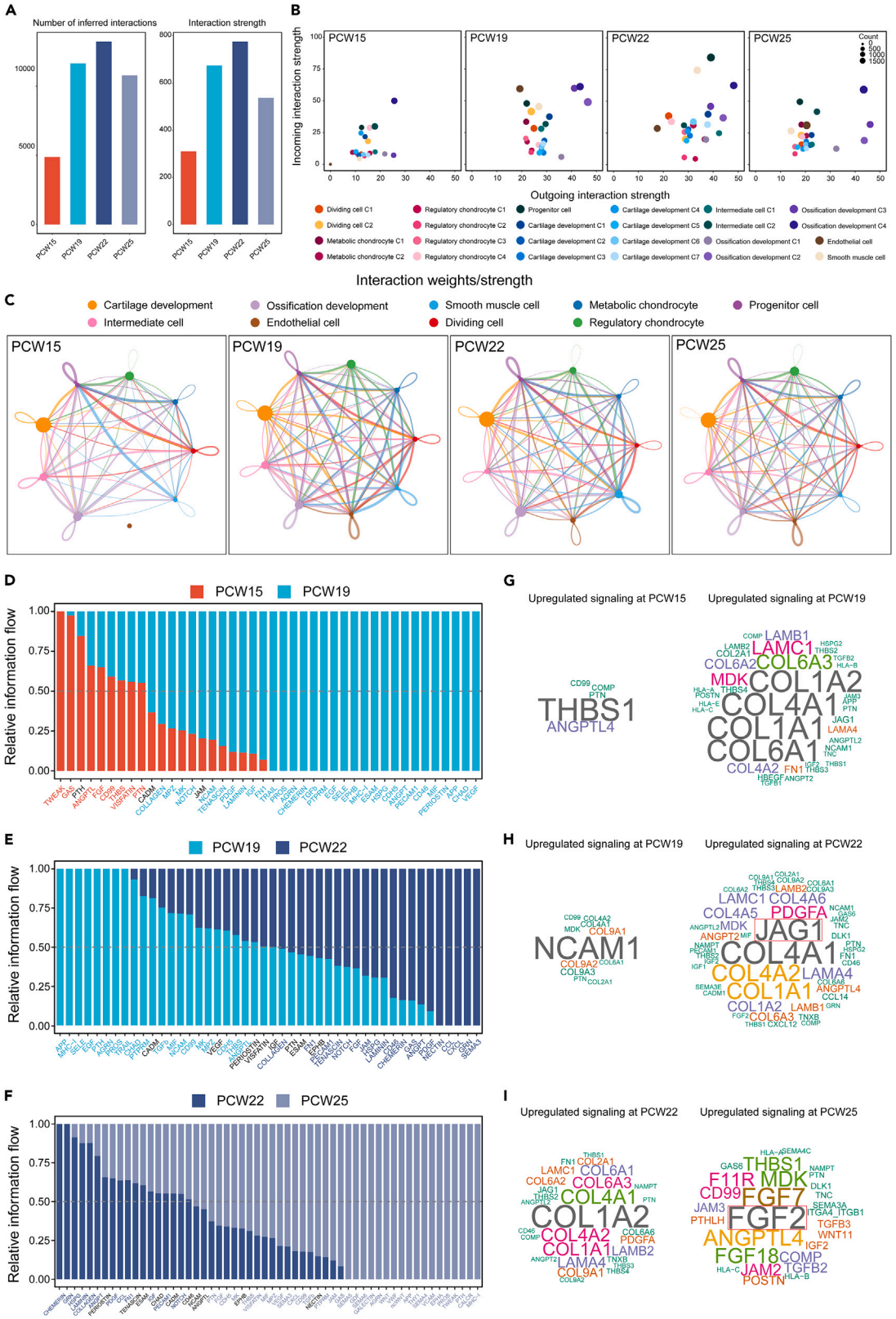
A
Number of inferred interactions
Interaction strength
PCW15
PCW19
PCW22
PCW25
B
Incoming interaction strength
Outgoing interaction strength
Count
Dividing cell C1
Dividing cell C2
Metabolic chondrocyte C1
Metabolic chondrocyte C2
Regulatory chondrocyte C1
Regulatory chondrocyte C2
Regulatory chondrocyte C3
Regulatory chondrocyte C4
Progenitor cell
Cartilage development C1
Cartilage development C2
Cartilage development C3
Cartilage development C4
Cartilage development C5
Cartilage development C6
Cartilage development C7
Intermediate cell C1
Intermediate cell C2
Ossification development C1
Ossification development C2
Ossification development C3
Ossification development C4
Endothelial cell
Smooth muscle cell
Interaction weights/strength
C
Cartilage development
Ossification development
Smooth muscle cell
Metabolic chondrocyte
Progenitor cell
Intermediate cell
Endothelial cell
Dividing cell
Regulatory chondrocyte
D
PCW15
PCW19
Relative information flow
E
PCW19
PCW22
F
PCW22
PCW25
G
Upregulated signaling at PCW15
Upregulated signaling at PCW19
H
Upregulated signaling at PCW19
Upregulated signaling at PCW22
I
Upregulated signaling at PCW22
Upregulated signaling at PCW25

Figure 6. Alterations in network structure and signaling strength of cell-cell communication inference during human fetal epiphyseal development

(A) Histograms of the number of inferred interactions and interaction strength in each sample.

(B) Dot plots of incoming and outgoing interaction strength color by cell subtypes.

(C) Circle plots of interaction weights/strengths of each population in each sample.

(D) Relative information flow of PCW19 compared with PCW15. Pathways with the same color as samples indicated significant upregulation.

(E) Relative information flow of PCW22 compared with PCW19. Pathways with the same color as samples indicated significant upregulation.

(F) Relative information flow of PCW25 compared with PCW22. Pathways with the same color as samples indicated significant upregulation.

(G) Word cloud showed upregulated signaling ligands at PCW15 (left) and upregulated signaling ligands at PCW19 (right). Word size indicates the extent of enrichment at PCW15 or PCW19.

(H) Word cloud showed upregulated signaling ligands at PCW19 (left) and upregulated signaling ligands at PCW22 (right). Word size indicates the extent of enrichment at PCW19 or PCW22. See Figures S11A–S11D.

(I) Word cloud showed upregulated signaling ligands at PCW22 (left) and upregulated signaling ligands at PCW25 (right). Word size indicates the extent of enrichment at PCW22 or PCW25. See Figures S11E and S11F.

subsequent states (Figure S9C). These results suggest that the intermediate cell population is a population with maturation similar to the cartilage or ossification development population rather than their ancestors.

The branch-specific gene analysis showed three distinct expression dynamics gene sets along branch 1 (Figure 5D). GO enrichment analysis revealed that genes in trajectory 1 are involved in cartilage condensation and cartilage development. And cells in trajectory 2 might implicate extracellular matrix organization, blood vessel development, and ossification (Figure 5E). In state 1, the expressions of *COL1A1* and *COL2A1* increased over time before reaching the first branch. After the first branch, the mRNA level of *COL1A1*, as well as *IGF1* and *POSTN*, kept increasing in trajectory 2 while decreasing in trajectory 1. On the contrary, the mRNA level of *COL2A1*, *ACAN*, and *COMP* increased in trajectory 1 while it decreased in trajectory 2 (Figures 5F and S9D).

The branch-specific gene analysis clustered three expression dynamics gene sets along branch 2 (Figure S9E). Nevertheless, genes with increasing expressions in trajectory 4 are also expressed in trajectory 3. GO enrichment analysis revealed that genes in trajectory 3 are involved in skeletal system development and cartilage development. And cells of pre-branch might implicate cell division (Figure S9F).

Next, the regulatory networks inference also showed distinct differential active regulons in states 2 and 4. Cells in state 2, constituted mainly by the cells from the ossification development population, exhibited high activity of *SHOX2*, *MAFB*, *HES1*, *NFIA*, and *JUNI* (Figures 5G and S9C). And in state 4, cells mainly came from the cartilage development population and exhibited high activity of known chondrogenesis regulators such as *SOX9* and *HIF1A*[38–40] (Figures 5G and S9C). These results further prove that the intermediate cell population with even distribution over this progress is related to cartilage and ossification development. Erythroblast transformation-specific (ETS) transcription factor ERG (*ERG*), a transcription factor with high expression and its high regulon activity mainly in the intermediate cell population, was elected to perform the immunofluorescent staining on the sagittal section of the epiphysis (Figures 5H and 5I). The ERG-positive cells were located close to the surface of the epiphysis and showed an increasing expression over development (Figures 5I and 5J). The IF co-staining showed the co-localization of ERG with its two downstream targets (GLI3 and SEMA3A) (Figures S10A and S10B). However, the protein expressions of GLI3 and SEMA3A increased gradually over development, and there was no decrease after the peak of gene expression showed in PCW19 from scRNA-seq (Figures S10C and S10D).

The human fetal epiphysis displays complex and dynamic cell-cell communication networks during development

The cell-cell communication networks underlying fetal epiphyseal development were inferred by using CellChat (version 1.4.0). CellChat infers the biologically significant cell-cell communication by assigning each ligand-receptor interaction with a probability value and performing a permutation test[41] (see STAR Methods). A subset of 3,000 cells randomly selected from each sample was analyzed separately. The total number and overall strength of inferred interactions within the epiphysis increased from PCW15 and peaked at PCW22 (Figure 6A). The incoming and outgoing interaction strength dynamically changed among every subtype during development (Figure 6B). The ossification development subtypes, including C2, C3, and C4, retained relatively higher incoming and outgoing interaction strength at each time course (Figure 6B). In most cases, self-interactions and inter-population interactions occurred continuously in early epiphyseal development, constructing complex cell-cell communication networks (Figure 6C).

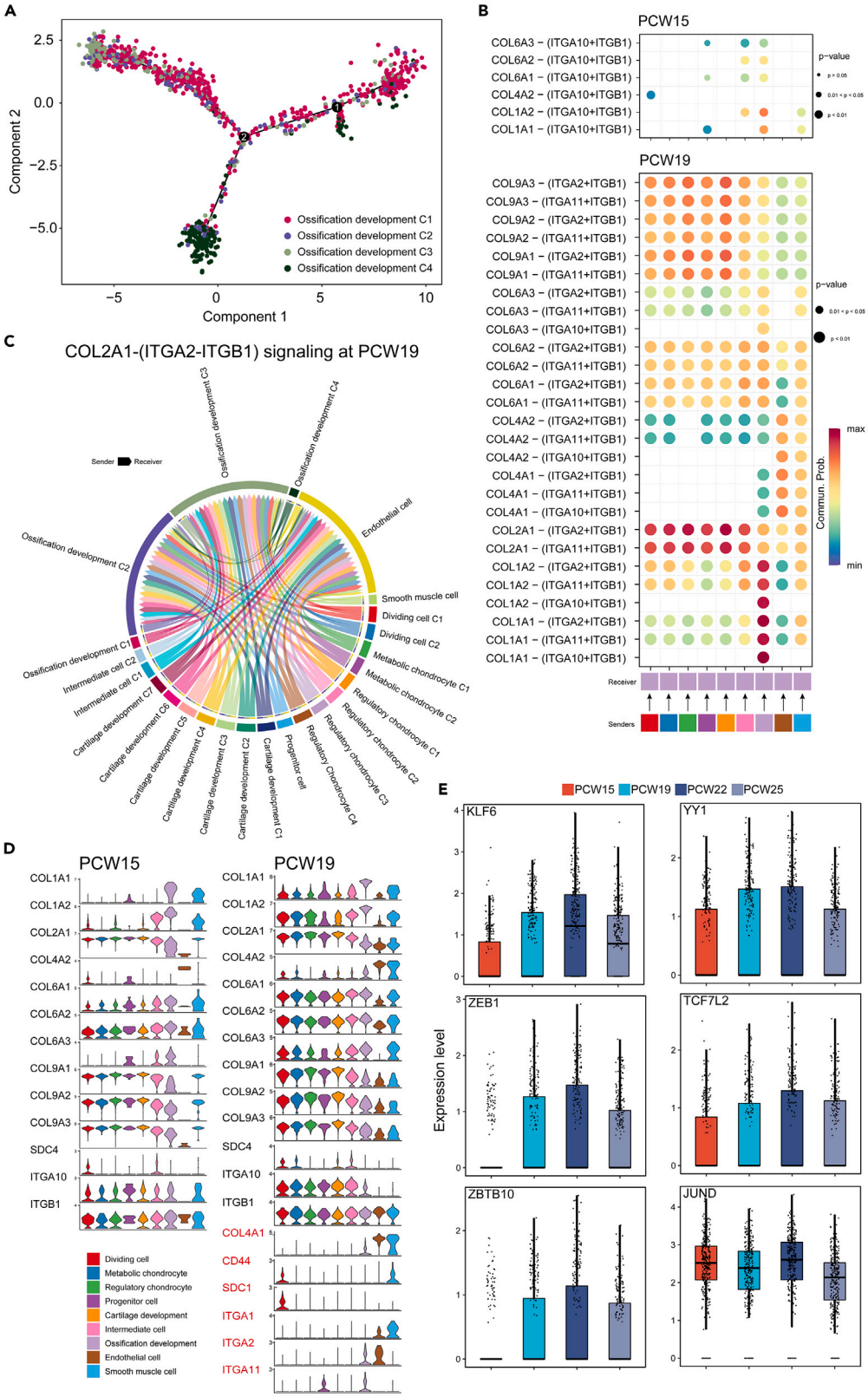
A
Component 2
Component 1
Ossification development C1
Ossification development C2
Ossification development C3
Ossification development C4
B
PCW15
PCW19
p−value
Commun. Prob.
max
min
Receiver
Senders
C
COL2A1-(ITGA2-ITGB1) signaling at PCW19
Sender
Receiver
Ossification development C3
Ossification development C4
Endothelial cell
Smooth muscle cell
Dividing cell C1
Dividing cell C2
Metabolic chondrocyte C1
Metabolic chondrocyte C2
Regulatory chondrocyte C1
Regulatory chondrocyte C2
Regulatory chondrocyte C3
Regulatory Chondrocyte C4
Progenitor cell
Cartilage development C1
Cartilage development C2
Cartilage development C3
Cartilage development C4
Cartilage development C5
Cartilage development C6
Cartilage development C7
Intermediate cell C1
Intermediate cell C2
Ossification development C1
Ossification development C2
D
PCW15
PCW19
COL1A1
COL1A2
COL2A1
COL4A2
COL6A1
COL6A2
COL6A3
COL9A1
COL9A2
COL9A3
SDC4
ITGA10
ITGB1
COL4A1
CD44
SDC1
ITGA1
ITGA2
ITGA11
Dividing cell
Metabolic chondrocyte
Regulatory chondrocyte
Progenitor cell
Cartilage development
Intermediate cell
Ossification development
Endothelial cell
Smooth muscle cell
E
PCW15 PCW19 PCW22 PCW25
KLF6
YY1
ZEB1
TCF7L2
ZBTB10
JUND
Expression level

Figure 7. Upregulated signaling correlated with the emergence of the Ossification development population

(A) Trajectory plots of the Ossification development population colored by subtypes.

(B) Dot plots of *COLLAGEN* signals received by the Ossification development population from other populations at PCW15 and PCW22. See Figure S12.

(C) Chord diagram of *COL2A1-(ITGA2-ITGB1)* signaling at PCW19.

(D) Stack violin plots of expressions of ligands and receptors correlating to *COLLAGEN* signaling in each population at PCW15 and PCW19. Genes in red were detected at PCW19 but not PCW15.

(E) Boxplots of predicted promoters/enhances (*KLF6*, *YY1*, *ZEB1*, *TCF7L2*, *ZBTB10*, and *JUND*) exhibited expression trends among each sample of the Ossification development population (Error bar represent mean ± SD).

The comparison results of samples at adjacent time points (PCW5 vs. PCW19, PCW19 vs. PCW22, PCW22 vs. PCW25) revealed significantly down- or upregulated information flows over the progress (See STAR Methods) (Figures 6D–6F).

At PCW19, the ligands involved in *COLLAGEN* signaling were strengthened compared to PCW15 (Figure 6G). Details of the *COLLAGEN* signaling alternation during development are investigated in the next section. At PCW22, *JAG1*-mediated *NOTCH* signaling was strengthened significantly (Figure 6H). From PCW19 to PCW22, *JAG1* and *NOTCH3* began to be expressed in some subtypes, indicating stronger interactions mediated by these correlating ligands and receptors (Figures S11A and S11B). The endothelial and smooth muscle cell populations, as senders and receivers, were engaged in all of the JAG1-mediated *NOTCH* signalings. Compared with other cell populations, the NOTCH singling target genes (HES5, HES7, HEY1, HEY2, MYC, and so on)[42] were mainly expressed in the endothelial and smooth muscle cell populations (Figure S11C). Compared to PCW19, the endothelial and smooth muscle cell populations of PCW22 tend to exhibit higher expression of NOTCH signaling targets (Figure S11C).

In the trajectory analysis of the ossification development population, GO enrichment analysis revealed that genes highly expressed in trajectory 3 (also state 4) are involved in tube development. Previous literature has reported that NOTCH signaling participates in the regulation of angiogenesis and endochondral ossification in bone.[43,44] Therefore, we observed the expression of ligands, receptors, and targets of NOTCH signal and endochondral ossification-related genes in PCW22 and PCW19 cells at state 4. These cells in PCW22 exhibited higher expression levels of NOTCH signaling-related genes, COL1A1, COL1A2, and endochondral ossification-related genes but lower COL2A1 than PCW19 (Figure S11D). These data indicate that NOTCH signaling may contribute to the ossification during early fetal epiphyseal development.

JAG1 is a known ligand capable of promoting angiogenesis via *NOTCH* signaling.[45] DLK1, with lower expressions in the ossification development population (Figure S11A), is another known ligand capable of regulating angiogenesis via *NOTCH* signaling.[46,47] These results suggested that NOTCH signaling may play a vital role in the development of cartilage canals. When it reached PCW25, *FGF2*-, *FGF7*-, and *FGF18*-mediated fibroblast growth factor (FGF) signalings were significantly upregulated (Figure 6I). *FGF7* and *FGF18* were found to be expressed mainly in the Ossfication development subtypes (Figure S11E). Moreover, the expression levels of *FGFR1* in the Ossfication development population were higher than those in the cartilage development population (Figure S11E). FGF family members play a role in cell survival, cell division, cell differentiation, and cell migration.[48] *FGF18* has been found as important regulators in the process of normal ossification and bone development.[49] In our cell-cell communication inference, the ossification development and intermediate cell populations received signals of *FGF2* as well as *FGF18* from other populations at PCW25 (Figure S11F).

Collectively, the analysis of cell-cell communication herein demonstrates a complex and dynamic intercellular network during human fetal epiphyseal development.

COL2A1-(ITGA2+ITGB1) and *COL2A1-(IGTA11+ITGB1)* signaling may implicate the emergence of the ossification development population

In the trajectory analysis of the ossification development population, cells in state 5 mainly came from C2 and C3 (Figures 4B and 7A). GO enrichment analysis of genes enriched in trajectory 4 indicated the cells in state 5 participated in GOBPs like trabecula formation and ossification (Figures 4C and 4E). Thus, focusing on the changes in signals received by these cells from others during development may reveal the mechanism involved in their emergence. The signals received by the ossification development population C3 changed obviously from PCW15 and PCW19 in terms of types and strength (Figures S12A–S12D). Among

these altered signals at PCW19, *COL2A1-(ITGA2+ITGB1)* and *COL2A1-(IGTA11+ITGB1)* signals, with maximum probability, were predicted to mediate interactions between *COL2A1* highly expressed populations and the ossification development population C3 (Figures 4B, S12A, and S12B). It is also the situation in the ossification development C2 (Figure 7C). *ITGA2* encodes an alpha integrin and forms a heterodimer with a beta subunit, functioning as a transmembrane receptor for collagens and related proteins.[50] Previous studies have reported that integrin receptors were able to mediate the master transcription factor *RUNX2* in osteoblast differentiation.[51] Interestingly, the expression of *ITGA2* and *ITGA11* was not detected in the ossification development population until PCW19 (Figure 7D). In addition, predicted promoters or enhancers of *ITGA2* (*KLF6*, *YY1*, *ZEB1*, *TCF7L2*, *ZBTB10*, and *JUND*)[52] showed a similar trend of increasing expression levels from PCW15 and peaking at PCW22 (Figure 7E). These results indicate that *COL2A1-(ITGA2+ITGB1)* and *COL2A1-(IGTA11+ITGB1)* signaling may implicate the emergence of the ossification development population.

DISCUSSION

In this study, we investigated the dynamic transcriptome changes during the development of early fetal epiphysis at the single-cell level. Our data demonstrate that epiphyseal cells contain multiple subtypes distinguished by specific markers, gene signatures, GO enrichment analysis, and GSVA. The analyses of cell trajectories, transcriptional regulatory networks, and intercellular communication described the alternation in transcriptional expression at this stage. Therefore, we constructed a sequence atlas of human fetal epiphyseal development, providing a panoramic dataset encompassing cell subtypes, cell trajectories, cell transcription regulatory networks, and intercellular communication. We also found that transcriptome expression has determined differentiation orientation to cartilage or ossification among the subtypes at this stage. Moreover, the ossification development population may play a vital role in cartilage canal formation at this stage and SOCs formation at the next stage. Our findings will advance the understanding of cell biological changes during epiphysis development.

During PCW15-PCW25, the epiphysis of the distal femur expands in size, inside which the cartilage canal appears.[6] Cartilage canals are cartilaginous tubes containing vessels, embedded in hyaline cartilage.[18,53] Consistent with these reports, we confirmed the existence of the populations of chondrocytes, endothelial, and smooth muscle cells. The endothelial and smooth muscle cells may contribute to the formation of vessels in the cartilage canals. We also observed the self-fluorescent red blood cells in the cartilage canals via digital sections, indicating interconnections with the circulatory system (Figure S1G). These results suggest vascular endothelial cells and smooth muscle cells may migrate from other areas to the epiphysis. However, the expression of HIF1A (around these canals) (Figure S4B) and *ANGPTL4* (in the endothelial cell at PCW25, data not shown) indicated it was still a hypoxia environment in the epiphysis. Further studies are needed to investigate the cellular biology underlying the emergence of cartilage canals.

In epiphysis, SOCs are considered the starting points of ossification.[8] Although the determinants of SOCs formation have not yet been fully elucidated, external vascular invasion and incorporation with cartilage canals were believed to be vital triggers.[54,55] The SOCs generally form at PCW28 in distal femoral epiphysis.[6] Our findings add to one opinion that transcriptome expression may have determined differentiation orientation toward cartilage or ossification before SOCs formation. We found that the expression levels of *COL1* (*COL1A1* and *COL1A2*) and *COL2* (*COL2A1* and *COL2A2*) were able to distinguish epiphyseal cells other than endothelial and smooth muscle cells, resulting in $COL2^{hi}COL1^{lo}$ cells with high expression of *COL2* and low expression of COL1, $COL2^{lo}COL1^{hi}$ cells with highly expressed *COL1* but lowly expressed *COL2*, and $COL2^{mo}COL1^{mo}$ cells with moderate expression of COL1 and *COL2* (Figures 1F and S12D). The organization of type I collagen is one of the significant steps during the early osteoblast differentiation and ossification.[56] Moreover, the GO enrichment analysis and GSVA indicated $COL2^{lo}COL1^{hi}$ cells engaged in tube morphogenesis, ossification, trabecula formation, and extracellular matrix organization (Figures 2B, 4E, S3, and S4, Table S5). Regulons correlating to bone development, such as *ALX4*, *TWIST1*, and *DLX2*,[57–59] were inferred to be differentially active in $COL2^{lo}COL1^{hi}$ cells by GRNs analysis (Figure 2E). Therefore, we speculate that a group of cells has committed toward ossification during early fetal epiphyseal development.

We further analyzed the development trajectory of this population and observed that cells are mainly distributed in two trajectories: trajectory 3 and trajectory 4 (Figure 4B). The highly expressed genes of trajectory 4 were enriched in bone trabecular formation, ossification, and biomineralization (Figures 4C and 4E) in GO analysis, suggesting that trajectory 4 may be more specifically related to ossification

development and osteogenic differentiation. The GRNs and expression analysis revealed NF-1 is one of the active transcription factor signals in trajectory 4 cells (also state 5 cells). The dynamic expression of *NFIA* in scRNA-seq data over development (Figure S6D), NF-1 in the IF staining over development (Figures 4G and 4I), and *NFIA* over *in vitro* osteogenic differentiation were consistent (Figures S8A and S8B). We also screened out two downstream targets of NF-1 (IGF-1 and ASPN). Both IGF-1 and ASPN have been reported to be involved in the process of osteoblast differentiation or collagen biomineralization.[60,61] We observed the co-localization of IGF-1 and ASPN with NF-1 and similar expression trends (Figure 4I and S8F). The consistent results from the IF co-localization assay and *in vitro* cell differentiation assay also fortify the findings acquired from scRNA-seq data (Figures S8A and S8B).

GO enrichment analysis revealed that highly expressed genes in trajectory 3 correlated with tube development (Figures 4C and 4E). It indicates that cells of trajectory 3 may contribute to the formation of cartilage canals. *FOSB* was one of the active transcriptional signals in trajectory 3. Both *LRP1* and ATF4 are downstream targets of *FOSB*. Previous studies have proved that both LRP1 and ATF4 regulate the process of osteogenesis.[60,61] ATF4, a transcription factor, is able to promote biomineralization via mTOR signaling.[61] We observed the co-localization of FOBS and its targets (LRP1 and ATF4) (Figures S7A and S7B). The expression of LRP1 and ATF4 increased over development (Figures S7C and S7D). The differentiation experiments also verified that the expression of *LRP1* will increase over osteogenesis (Figure S7H). We also detected the expression of other downstream genes of *FOSB* in osteogenic differentiation, including *FN1*, *KLF6*, *MAPRE2*, *COL3A1*, and *LIMA1*. These genes also showed an increasing trend over early osteogenesis. These results suggest that the cells in trajectory 3 are involved not only in tube formation but also in the regulation of osteogenic differentiation. Collectively, these $COL2^{lo}COL1^{hi}$ cells may play a key role in cartilage canals and SOCs formation.

To find out the clues to the mechanism of the emergence of the ossification development population, we performed a cell-cell communication analysis. We found that signals *COL2A1-(ITGA2+ITGB1)* and *COL2A1-(ITGA11+ITGB1)* elevated between the ossification development population C3 (receiver) and the other $COL2^{hi}COL1^{lo}$ cells (senders) after PCW15 (Figure S12). Since epiphysis originates from cartilage development, we speculate that the formation of type 2 collagen is earlier than that of type 1 collagen. The proportion of the ossification development subtypes at PCW15-PCW25 also supports speculation (Figure 1D). Thus, the expression of receptors (*ITGA2+ITGB1* or *ITGA11+ITGB1*) may be the key to the presence of the ossification development population. *ITGB1* was expressed in most cells since PCW15. However, the expression of *ITGA2* and *ITGA11* was not detected in the ossification development population until PCW19 (Figure 7D). Moreover, some promoters or enhancers predicted to modify *ITGA2* also exhibit increased expression in this population from PCW15 to PCW22 (Figure 7E). Together with *ITGB1*, *ITGA2* or *ITGA11* forms an integrin receptor, receiving signals from $COL2^{hi}COL1^{lo}$ cells via binding to *COL2A1*. It has been reported that *COL2A1-(ITGA2+ITGB1)* and *COL2A1-(ITGA11+ITGB1)* signalings were implicated in mediating the master transcription factor *RUNX2* in osteoblast differentiation.[62] Collectively, the emergence of the ossification development population may correlate with the expression of *ITGA2* and *ITGA11*. However, the mechanism underlying the presence of *ITGA2* or *ITGA11* in these cells remains unclear. Further epigenetic studies may help to answer this question.

We also identified $COL2^{mo}COL1^{mo}$ cells with moderate expression of *COL1* and *COL2*. Indeed, the expression levels of *COL4A2*, *COL6* (*COL6A1*, *COL6A2*, and *COL6A3*), and *COL9* (*COL9A1*, *COL9A2*, and *COL9A3*) in $COL2^{mo}COL1^{mo}$ cells were also between those in $COL2^{hi}COL1^{lo}$ and $COL2^{lo}COL1^{hi}$ cells (Figure 7D). *COL10A1* was not detected among these cells, indicating that they are not likely hypertrophic chondrocytes.[63–65] Trajectory analysis indicated that the $COL2^{mo}COL1^{mo}$ cells were not the ancestor of the Ossification and cartilage development populations. $COL2^{mo}COL1^{mo}$ cells were distributed evenly in all trajectories, suggesting that they might correlate with ossification and cartilage development (Figure 5C). Therefore, we thought the population of $COL2^{mo}COL1^{mo}$ cells was an intermediate state between ossification and cartilage development rather than an independent one. Thus, we named it the intermediate cell population. When analyzing the transcriptional regulatory signals, we found that most active regulons of the intermediate cell population overlapped with those of the cartilage and ossification development populations (Figure 2E). We screened out a transcription factor *ERG*, which was highly expressed in the intermediate cell population but not in the cartilage and ossification development populations (Figure 5H). ERG is a member of the *ETS* family of transcription factors. It is key to embryonic development, cell proliferation, differentiation, angiogenesis, inflammation, and apoptosis.[66] We found that ERG protein was expressed highly in the cells close to the epiphyseal surface (Figure 5I). GLI3 and SEMA3A, downstream

targets of ERG, were co-localized with ERG (Figures S10A and S10B). Both of these two genes are reported to be involved in the development of the skeletal system.[67–69] However, the difference is that the protein expression levels of GLI3 and SEMA3A continue to increase over development, and there is no peak situation like the existence of genes (Figures S10C and S10D). This result may be related to the lag between protein translation and gene transcription, the rate of protein degradation, or the diverse network of gene regulation. It has been reported that hypertrophic chondrocyte was able to transdifferentiate to osteoblast.[65] However, we tend to believe that the intermediate cell population is different from hypertrophic chondrocytes as it does not express *COL10A1* (Figure 7D). Thus, the distribution and function of the intermediate cell still need validation through means of biological experiments in lineage study.

Chondrocytes can be classified not only into hyaline chondrocytes, hypertrophic chondrocytes, and fibrochondrocytes according to their morphology and distribution but also into proliferative chondrocytes, effector chondrocytes, regulatory chondrocyte, and homeostatic chondrocytes according to their single-cell transcriptome characteristics.[64] We identified 16 subtypes of $COL2^{hi}COL1^{lo}$ cells in this study. Among these subtypes, two engaged in cell division, two in the metabolism of metal ions or pyruvate, four in regulating nitrogen compounds, cell adhesion, or cell proliferation, and seven in extracellular matrix synthesis and cartilage development (Figure S2). One population exhibited similar markers expression to skeletal stem cells identified from the growth plate[70] (Figure 1G). The seven subtypes engaged in extracellular matrix synthesis and cartilage development may play a central role in the organization of the cartilaginous matrix during epiphyseal development. Thus, we named them the cartilage development populations C1-C7. These cells went through one branch and formed two trajectories during development (Figure 3B). The evidence that most cells developed along trajectory 1 with enriched genes engaged in cartilage development implies that the formation of the structural epiphysis may potentially be a consequence of the development of these populations. A key contribution of our atlas is providing a dynamic transcriptome featuring the fetal epiphyseal development.

Single-cell trajectory analysis revealed the cartilage development population passed through one branchpoint, dividing into trajectory 1 and trajectory 2. Most cells were distributed in trajectory 1 (Figure 3B). HIF1A is one of the active transcriptional signals of trajectory 1. We examined the co-localization and temporal expression of HIF1A and its downstream target protein MIG-6. MIG-6-positive cells also existed around the cartilage canals (Figure S4D). HIF1A participates in the cartilage differentiation process during limb development.[71] YBX1, one of the active transcriptional signals of the initial state (Figure 3B), is reported to modulate chondrogenesis process.[72] We screened out two downstream targets of YB-1 (CALR and CD63) and observed their co-localization (Figures S5A and S5B). CALR has been found to play a role for endoplasmic reticulum calcium signaling via calreticulin in the differentiation of embryonic stem cells (ESCs) to closely associated osteoblast or chondrocyte lineages.[73] However, although the protein expression of CALR and CD63 decreased gradually after PCW12, which is consistent with the analysis results of their scRNA-seq data, their expression increased again during PCW27 $\sim$ 32, while the expression of CALR and CD63 decreased over the early chondrogenesis and increased laterally (Figure S5G). We are still uncertain about the cause of the lateral increase of these targets and consider further experiments to investigate it. The consistent dynamic expression of YBX1 and its downstream targets (*HNRNPA2B1*, *EIF5A*, *COPE*, and *ACTG1*) between scRNA-seq data and chondrogenic differentiation also fortify the findings over cartilage development from scRNA-seq analysis (Figures S5G and S5H).

The analysis of cell-cell communication reveals that the interactions between cell populations are complex and dynamic during epiphyseal development. Generally, ossification development, endothelium, and smooth muscle cell populations participate in more intercellular interaction than others, suggesting that these cells are in a more active state at this stage (Figure 6B).

Our results also demonstrate that the *NOTCH* signaling pathway may play a vital role in cartilage canal formation. DLK1 and JAG1 have been reported to be involved in regulating angiogenesis through the NOTCH signaling pathway.[45–47] These genes were found to be expressed in the fetal epiphysis (Figure S11A). The targets of the *NOTCH* signaling pathway, including *HES1*, *HES5*, and *HES7* in the *HES* family, *HEY1*, *HEY2*, and *HEYL* in the *HESR* family, and the targets of the *NOTCH* signaling pathway reported in other literature, were also concentrated in endothelial cell population and smooth muscle cell population[42] (Figure S11C). Compared with PCW19, the expression of most NOTCH signaling target genes in the smooth muscle cell population in the PCW22 is higher (Figure S11C). According to the composition of cartilage canals, we speculate that the *NOTCH* signaling pathway may contribute to the formation of cartilage canals.

In a murine study, *NOTCH* signaling is found to play a role in promoting angiogenesis and osteogenesis in bone.[43,44] GO enrichment analysis revealed that highly expressed genes in trajectory 3 correlated with tube development (Figures 4C and 4E). These cells are all $COL2^{lo}COL1^{hi}$ cells (Figure 4B). In addition, PCW22 is higher than PCW19 in a proportion of cells in trajectory 3 (Figure 4B). Among these cells in trajectory 3, the *NOTCH* signaling-related genes and the endochondral ossification-related genes exhibited higher expression in PCW22 than in PCW19 (Figure S11D). Therefore, we speculate that the *NOTCH* signal may also participate in the development of ossification in epiphysis during this period. However, the verification of this process requires further research by means of diverse biological experiments.

Limitation of the study

The findings and predictions in this study are based on scRNA-seq, trajectory, GRNs, and cell-cell communication inference and are limited by the cell quality, capture rate, machine sensitivity, and algorithm optimization degree. We could not assess the effects of the mother's age, nutritional status, medications used, pregnant environment, and time post-death. In addition, a potential interpretation of the cellular and gene expression patterns identified between the different time points could be that samples come from different subjects and there is inter-subject variability. Also, the cell-cell communication analysis gives the possibility of indicated ligand-receptor pairs, and many more experiments will be needed to demonstrate the situation of cell-cell communication. Furthermore, the sample size and small epiphyseal tissue of an early fetus will lead to a low number of captured cells, which may lead to the loss of biological information. Epiphyseal development lasts from embryo to adolescence. Our data do not reflect the whole process of epiphyseal development but only some stages.

In order to confirm the development process of epiphyseal cells in the earlier and later stages, such as the earliest appearance time of the ossification development population, the functional differentiation time of chondrocytes, and the relationship between the appearance of SOCs and these cells at this stage, it is still necessary to supplement a large number of samples and data for analysis and functional verifications.

STAR★METHODS

Detailed methods are provided in the online version of this paper and include the following:

- KEY RESOURCES TABLE
- RESOURCE AVAILABILITY
  - Lead contact
  - Materials availability
  - Data and code availability
- EXPERIMENTAL MODEL AND STUDY PARTICIPANT DETAILS
  - Human tissue
- METHOD DETAILS
  - scRNA-SEQ samples preparation
  - scRNA-SEQ
  - scRNA-SEQ data analysis
  - Cell culture
  - Chondrogenesis differentiation
  - Osteogenesis differentiation
  - Cell staining and capture
  - RNA extraction, purification and reverse transcription
  - Quantitative real-time PCR (qPCR)
  - Paraffin sections and IF staining
- QUANTIFICATION AND STATISTICAL ANALYSIS

SUPPLEMENTAL INFORMATION

Supplemental information can be found online at https://doi.org/10.1016/j.isci.2023.107200.

ACKNOWLEDGMENTS

We gratefully acknowledge the Obstetrics Department of Southern Hospital of Southern Medical University and the Obstetrics Department of Taihe Branch of Southern Hospital for their assistance in the process of tissue separation. We appreciate the assistance from Nachun Chen and Xiaoyu Li for tissue preparation.

We would like to thank the Central Laboratory of Southern Hospital of Southern Medical University (Bingyi Wu, Xiaolan Zhang, Xiaojing Wang, Guo Yin) for providing us with access to a tissue microtome, fluorescence microscope, capture system, cell culture equipments, and PCR machines. We thank Yuanxin Company (Qiang Li) for its help in sequencing single-cell transcriptomes. This work was funded by the National Natural Science Foundation of China (no.31771051, L.Z. and no.82071669, L.H.), Natural Science Foundation of Guangdong Province (no.2018B030311041, L.Z.), and Science and Technology Project of Guangzhou City (no.201803010114, L.Z.).

AUTHOR CONTRIBUTIONS

Conceptualization, L.H. and L.Z.; Methodology, L.H. and L.Z.; Validation, L.B.; Formal analysis, Z.D., Z.L., Y.J., and X.Z.; Investigation, Z.D., S.R., L.G., F.W., Z.F., Y.W., R.C., and Y.J.; Resources, L.B., F.C., Y.Z., and L.H.; Writing – Original Draft, Z.D. and L.B.; Writing – Review & Editing, Z.D., S.R., L.G., F.W., S.F., L.H., and L.Z.; Visualization, Z.D., S.R., L.G., and F.W.; Supervision, L.Z.; Project administration, L.Z.; Funding acquisition, L.H. and L.Z.

DECLARATION OF INTERESTS

The authors declare no competing interests.

INCLUSION AND DIVERSITY

We support inclusive, diverse, and equitable conduct of research.

Received: December 15, 2022
Revised: May 18, 2023
Accepted: June 20, 2023
Published: June 24, 2023

REFERENCES

1. Setiawati, R., and Rahardjo, P. (2018). Bone Development and Growth (IntechOpen). https://doi.org/10.5772/intechopen.82452.

2. Hecht, J.T., Nelson, L.D., Crowder, E., Wang, Y., Elder, F.F., Harrison, W.R., Francomano, C.A., Prange, C.K., Lennon, G.G., and Deere, M. (1995). Mutations in exon 17B of cartilage oligomeric matrix protein (COMP) cause pseudoachondroplasia. Nat. Genet. *10*, 325–329. https://doi.org/10.1038/ng0795-325.

3. Briggs, M.D., Hoffman, S.M., King, L.M., Olsen, A.S., Mohrenweiser, H., Leroy, J.G., Mortier, G.R., Rimoin, D.L., Lachman, R.S., and Gaines, E.S. (1995). Pseudoachondroplasia and multiple epiphyseal dysplasia due to mutations in the cartilage oligomeric matrix protein gene. Nat. Genet. *10*, 330–336. https://doi.org/10.1038/ng0795-330.

4. Olsen, B.R., Reginato, A.M., and Wang, W. (2000). Bone development. Annu. Rev. Cell Dev. Biol. *16*, 191–220. https://doi.org/10.1146/annurev.cellbio.16.1.191.

5. Bradley, E.W., Carpio, L.R., van Wijnen, A.J., McGee-Lawrence, M.E., and Westendorf, J.J. (2015). Histone Deacetylases in Bone Development and Skeletal Disorders. Physiol. Rev. *95*, 1359–1381. https://doi.org/10.1152/physrev.00004.2015.

6. Suzuki, Y., Matsubayashi, J., Ji, X., Yamada, S., Yoneyama, A., Imai, H., Matsuda, T., Aoyama, T., and Takakuwa, T. (2019). Morphogenesis of the femur at different stages of normal human development. PLoS One *14*, e0221569. https://doi.org/10.1371/journal.pone.0221569.

7. Varich, L.J., Laor, T., and Jaramillo, D. (2000). Normal maturation of the distal femoral epiphyseal cartilage: age-related changes at MR imaging. Radiology *214*, 705–709. https://doi.org/10.1148/radiology.214.3.r00mr20705.

8. Xie, M., and Chagin, A.S. (2021). The epiphyseal secondary ossification center: Evolution, development and function. Bone *142*, 115701. https://doi.org/10.1016/j.bone.2020.115701.

9. Roach, H.I., Baker, J.E., and Clarke, N.M. (1998). Initiation of the bony epiphysis in long bones: chronology of interactions between the vascular system and the chondrocytes. J. Bone Miner. Res. *13*, 950–961. https://doi.org/10.1359/jbmr.1998.13.6.950.

10. Cole, H.A., Yuasa, M., Hawley, G., Cates, J.M.M., Nyman, J.S., and Schoenecker, J.G. (2013). Differential development of the distal and proximal femoral epiphysis and physis in mice. Bone *52*, 337–346. https://doi.org/10.1016/j.bone.2012.10.011.

11. Connolly, S.A., Jaramillo, D., Hong, J.K., and Shapiro, F. (2004). Skeletal development in fetal pig specimens: MR imaging of femur with histologic comparison. Radiology *233*, 505–514. https://doi.org/10.1148/radiol.2332030131.

12. Xie, M., Gol'din, P., Herdina, A.N., Estefa, J., Medvedeva, E.V., Li, L., Newton, P.T., Kotova, S., Shavkuta, B., Saxena, A., et al. (2020). Secondary ossification center induces and protects growth plate structure. Elife *9*, e55212. https://doi.org/10.7554/eLife.55212.

13. Jans, L.B.O., Jaremko, J.L., Ditchfield, M., and Verstraete, K.L. (2011). Evolution of femoral condylar ossification at MR imaging: frequency and patient age distribution. Radiology *258*, 880–888. https://doi.org/10.1148/radiol.10101103.

14. Tong, W., Tower, R.J., Chen, C., Wang, L., Zhong, L., Wei, Y., Sun, H., Cao, G., Jia, H., Pacifici, M., et al. (2019). Periarticular Mesenchymal Progenitors Initiate and Contribute to Secondary Ossification Center Formation During Mouse Long Bone Development. Stem Cell. *37*, 677–689. https://doi.org/10.1002/stem.2975.

15. Heinonen, J., Zhang, F.-P., Surmann-Schmitt, C., Honkala, S., Stock, M., Poutanen, M., and Säämänen, A.M. (2017). Defects in chondrocyte maturation and secondary ossification in mouse knee joint epiphyses due to Snorc deficiency. Osteoarthritis Cartilage *25*, 1132–1142. https://doi.org/10.1016/j.joca.2017.03.010.

16. Rivas, R., and Shapiro, F. (2002). Structural stages in the development of the long bones and epiphyses: a study in the New Zealand white rabbit. J. Bone Joint Surg. Am. *84*, 85–100. https://doi.org/10.2106/00004623-200201000-00013.

17. Alvarez, J., Costales, L., Serra, R., Balbín, M., and López, J.M. (2005). Expression patterns of matrix metalloproteinases and vascular endothelial growth factor during epiphyseal ossification. J. Bone Miner. Res. *20*, 1011–1021. https://doi.org/10.1359/JBMR.050204.

18. Blumer, M.J.F., Longato, S., Richter, E., Pérez, M.T., Konakci, K.Z., and Fritsch, H. (2005). The role of cartilage canals in endochondral and perichondral bone formation: are there similarities between these two processes? J. Anat. *206*, 359–372. https://doi.org/10.1111/j.1469-7580.2005.00404.x.

19. van Bruggen, D., Pohl, F., Langseth, C.M., Kukanja, P., Lee, H., Albiach, A.M., Kabbe, M., Meijer, M., Linnarsson, S., Hilscher, M.M., et al. (2022). Developmental landscape of human forebrain at a single-cell level identifies early waves of oligodendrogenesis. Dev. Cell *57*, 1421–1436.e5. https://doi.org/10.1016/j.devcel.2022.04.016.

20. Ge, W., Tan, S.-J., Wang, S.-H., Li, L., Sun, X.-F., Shen, W., and Wang, X. (2020). Single-cell Transcriptome Profiling reveals Dermal and Epithelial cell fate decisions during Embryonic Hair Follicle Development. Theranostics *10*, 7581–7598. https://doi.org/10.7150/thno.44306.

21. Byrnes, L.E., Wong, D.M., Subramaniam, M., Meyer, N.P., Gilchrist, C.L., Knox, S.M., Tward, A.D., Ye, C.J., and Sneddon, J.B. (2018). Lineage dynamics of murine pancreatic development at single-cell resolution. Nat. Commun. *9*, 3922. https://doi.org/10.1038/s41467-018-06176-3.

22. Hao, Y., Hao, S., Andersen-Nissen, E., Mauck, W.M., Zheng, S., Butler, A., Lee, M.J., Wilk, A.J., Darby, C., Zager, M., et al. (2021). Integrated analysis of multimodal single-cell data. Cell *184*, 3573–3587.e29. https://doi.org/10.1016/j.cell.2021.04.048.

23. Yi, S.W., Kim, H.J., Oh, H.J., Shin, H., Lee, J.S., Park, J.S., and Park, K.-H. (2018). Gene expression profiling of chondrogenic differentiation by dexamethasone-conjugated polyethyleneimine with SOX trio genes in stem cells. Stem Cell Res. Ther. *9*, 341. https://doi.org/10.1186/s13287-018-0998-7.

24. Wu, C.-L., Dicks, A., Steward, N., Tang, R., Katz, D.B., Choi, Y.-R., and Guilak, F. (2021). Single cell transcriptomic analysis of human pluripotent stem cell chondrogenesis. Nat. Commun. *12*, 362. https://doi.org/10.1038/s41467-020-20598-y.

25. Song, H., and Park, K.-H. (2020). Regulation and function of SOX9 during cartilage development and regeneration. Semin. Cancer Biol. *67*, 12–23. https://doi.org/10.1016/j.semcancer.2020.04.008.

26. Kalucka, J., de Rooij, L.P.M.H., Goveia, J., Rohlenova, K., Dumas, S.J., Meta, E., Conchinha, N.V., Taverna, F., Teuwen, L.-A., Veys, K., et al. (2020). Single-Cell Transcriptome Atlas of Murine Endothelial Cells. Cell *180*, 764–779.e20. https://doi.org/10.1016/j.cell.2020.01.015.

27. Li, Y., Ren, P., Dawson, A., Vasquez, H.G., Ageedi, W., Zhang, C., Luo, W., Chen, R., Li, Y., Kim, S., et al. (2020). Single-Cell Transcriptome Analysis Reveals Dynamic Cell Populations and Differential Gene Expression Patterns in Control and Aneurysmal Human Aortic Tissue. Circulation *142*, 1374–1388. https://doi.org/10.1161/CIRCULATIONAHA.120.046528.

28. Tikhonova, A.N., Dolgalev, I., Hu, H., Sivaraj, K.K., Hoxha, E., Cuesta-Domínguez, Á., Pinho, S., Akhmetzyanova, I., Gao, J., Witkowski, M., et al. (2019). The bone marrow microenvironment at single-cell resolution. Nature *569*, 222–228. https://doi.org/10.1038/s41586-019-1104-8.

29. Hänzelmann, S., Castelo, R., and Guinney, J. (2013). GSVA: gene set variation analysis for microarray and RNA-seq data. BMC Bioinf. *14*, 7. https://doi.org/10.1186/1471-2105-14-7.

30. Van de Sande, B., Flerin, C., Davie, K., De Waegeneer, M., Hulselmans, G., Aibar, S., Seurinck, R., Saelens, W., Cannoodt, R., Rouchon, Q., et al. (2020). A scalable SCENIC workflow for single-cell gene regulatory network analysis. Nat. Protoc. *15*, 2247–2276. https://doi.org/10.1038/s41596-020-0336-2.

31. Aibar, S., González-Blas, C.B., Moerman, T., Huynh-Thu, V.A., Imrichova, H., Hulselmans, G., Rambow, F., Marine, J.-C., Geurts, P., Aerts, J., et al. (2017). SCENIC: single-cell regulatory network inference and clustering. Nat. Methods *14*, 1083–1086. https://doi.org/10.1038/nmeth.4463.

32. Trapnell, C., Cacchiarelli, D., Grimsby, J., Pokharel, P., Li, S., Morse, M., Lennon, N.J., Livak, K.J., Mikkelsen, T.S., and Rinn, J.L. (2014). The dynamics and regulators of cell fate decisions are revealed by pseudotemporal ordering of single cells. Nat. Biotechnol. *32*, 381–386. https://doi.org/10.1038/nbt.2859.

33. Qiu, X., Hill, A., Packer, J., Lin, D., Ma, Y.-A., and Trapnell, C. (2017). Single-cell mRNA quantification and differential analysis with Census. Nat. Methods *14*, 309–315. https://doi.org/10.1038/nmeth.4150.

34. Fahrner, J.A., Lin, W.-Y., Riddle, R.C., Boukas, L., DeLeon, V.B., Chopra, S., Lad, S.E., Luperchio, T.R., Hansen, K.D., and Bjornsson, H.T. (2019). Precocious chondrocyte differentiation disrupts skeletal growth in Kabuki syndrome mice. JCI Insight *4*, 129380. https://doi.org/10.1172/jci.insight.129380.

35. Wu, X., Wang, X., Shan, L., Zhou, J., Zhang, X., Zhu, E., Yuan, H., and Wang, B. (2021). High-mobility group AT-Hook 1 mediates the role of nuclear factor I/X in osteogenic differentiation through activating canonical Wnt signaling. Stem Cell. *39*, 1349–1361. https://doi.org/10.1002/stem.3418.

36. Yuan, H., Li, M., Feng, X., Zhu, E., and Wang, B. (2021). miR-142a-5p promoted osteoblast differentiation via targeting nuclear factor IA. J. Cell. Physiol. *236*, 1810–1821. https://doi.org/10.1002/jcp.29963.

37. Becht, E., McInnes, L., Healy, J., Dutertre, C.-A., Kwok, I.W.H., Ng, L.G., Ginhoux, F., and Newell, E.W. (2018). Dimensionality reduction for visualizing single-cell data using UMAP. Nat. Biotechnol. *37*, 38–44. https://doi.org/10.1038/nbt.4314.

38. Oldershaw, R.A., Baxter, M.A., Lowe, E.T., Bates, N., Grady, L.M., Soncin, F., Brison, D.R., Hardingham, T.E., and Kimber, S.J. (2010). Directed differentiation of human embryonic stem cells toward chondrocytes. Nat. Biotechnol. *28*, 1187–1194. https://doi.org/10.1038/nbt.1683.

39. Lefebvre, V., Huang, W., Harley, V.R., Goodfellow, P.N., and de Crombrugghe, B. (1997). SOX9 is a potent activator of the chondrocyte-specific enhancer of the pro alpha1(II) collagen gene. Mol. Cell Biol. *17*, 2336–2346. https://doi.org/10.1128/MCB.17.4.2336.

40. Stegen, S., Laperre, K., Eelen, G., Rinaldi, G., Fraisl, P., Torrekens, S., Van Looveren, R., Loopmans, S., Bultynck, G., Vinckier, S., et al. (2019). HIF-1α metabolically controls collagen synthesis and modification in chondrocytes. Nature *565*, 511–515. https://doi.org/10.1038/s41586-019-0874-3.

41. Jin, S., Guerrero-Juarez, C.F., Zhang, L., Chang, I., Ramos, R., Kuan, C.-H., Myung, P., Plikus, M.V., and Nie, Q. (2021). Inference and analysis of cell-cell communication using CellChat. Nat. Commun. *12*, 1088. https://doi.org/10.1038/s41467-021-21246-9.

42. Borggrefe, T., and Oswald, F. (2009). The Notch signaling pathway: transcriptional regulation at Notch target genes. Cell. Mol. Life Sci. *66*, 1631–1646. https://doi.org/10.1007/s00018-009-8668-7.

43. Ramasamy, S.K., Kusumbe, A.P., Wang, L., and Adams, R.H. (2014). Endothelial Notch activity promotes angiogenesis and osteogenesis in bone. Nature *507*, 376–380. https://doi.org/10.1038/nature13146.

44. Xu, C., Dinh, V.V., Kruse, K., Jeong, H.-W., Watson, E.C., Adams, S., Berkenfeld, F., Stehling, M., Rasouli, S.J., Fan, R., et al. (2022). Induction of osteogenesis by bone-targeted Notch activation. Elife *11*, e60183. https://doi.org/10.7554/eLife.60183.

45. Benedito, R., Roca, C., Sörensen, I., Adams, S., Gossler, A., Fruttiger, M., and Adams, R.H. (2009). The notch ligands Dll4 and Jagged1 have opposing effects on angiogenesis. Cell *137*, 1124–1135. https://doi.org/10.1016/j.cell.2009.03.025.

46. Huang, C.-C., Kuo, H.-M., Wu, P.-C., Cheng, S.-H., Chang, T.-T., Chang, Y.-C., Kung, M.-L., Wu, D.-C., Chuang, J.-H., and Tai, M.-H. (2018). Soluble delta-like 1 homolog (DLK1) stimulates angiogenesis through Notch1/Akt/eNOS signaling in endothelial cells. Angiogenesis *21*, 299–312. https://doi.org/10.1007/s10456-018-9596-7.

47. Rodríguez, P., Higueras, M.A., González-Rajal, A., Alfranca, A., Fierro-Fernández, M., García-Fernández, R.A., Ruiz-Hidalgo, M.J., Monsalve, M., Rodríguez-Pascual, F., Redondo, J.M., et al. (2012). The non-canonical NOTCH ligand DLK1 exhibits a novel vascular role as a strong inhibitor of angiogenesis. Cardiovasc. Res. *93*, 232–241. https://doi.org/10.1093/cvr/cvr296.

48. Beenken, A., and Mohammadi, M. (2009). The FGF family: biology, pathophysiology and therapy. Nat. Rev. Drug Discov. *8*, 235–253. https://doi.org/10.1038/nrd2792.

49. Cinque, L., Forrester, A., Bartolomeo, R., Svelto, M., Venditti, R., Montefusco, S., Polishchuk, E., Nusco, E., Rossi, A., Medina, D.L., et al. (2015). FGF signalling regulates bone growth through autophagy. Nature *528*, 272–275. https://doi.org/10.1038/nature16063.

50. Rubel, D., Frese, J., Martin, M., Leibnitz, A., Girgert, R., Miosge, N., Eckes, B., Müller, G.A., and Gross, O. (2014). Collagen receptors integrin alpha2beta1 and discoidin domain receptor 1 regulate maturation of the glomerular basement membrane and loss of integrin alpha2beta1 delays kidney fibrosis in COL4A3 knockout mice. Matrix Biol. *34*, 13–21. https://doi.org/10.1016/j.matbio.2014.01.006.

51. Schneider, G.B., Zaharias, R., and Stanford, C. (2001). Osteoblast integrin adhesion and signaling regulate mineralization. J. Dent. Res. *80*, 1540–1544. https://doi.org/10.1177/00220345010800061201.

52. Fishilevich, S., Nudel, R., Rappaport, N., Hadar, R., Plaschkes, I., Iny Stein, T., Rosen, N., Kohn, A., Twik, M., Safran, M., et al. (2017). GeneHancer: genome-wide integration of enhancers and target genes in GeneCards. Database *2017*, bax028. https://doi.org/10.1093/database/bax028.

53. Blumer, M.J.F., Longato, S., and Fritsch, H. (2008). Structure, formation and role of cartilage canals in the developing bone. Ann. Anat. *190*, 305–315. https://doi.org/10.1016/j.aanat.2008.02.004.

54. Finnøy, A., Olstad, K., and Lilledahl, M.B. (2017). Non-linear optical microscopy of cartilage canals in the distal femur of young pigs may reveal the cause of articular osteochondrosis. BMC Vet. Res. *13*, 270. https://doi.org/10.1186/s12917-017-1197-y.

55. Olstad, K., Hendrickson, E.H.S., Carlson, C.S., Ekman, S., and Dolvik, N.I. (2013). Transection of vessels in epiphyseal cartilage canals leads to osteochondrosis and osteochondrosis dissecans in the femoro-patellar joint of foals; a potential model of juvenile osteochondritis dissecans. Osteoarthritis Cartilage *21*, 730–738. https://doi.org/10.1016/j.joca.2013.02.005.

56. Huang, W., Yang, S., Shao, J., and Li, Y.-P. (2007). Signaling and transcriptional regulation in osteoblast commitment and differentiation. Front. Biosci. *12*, 3068–3092. https://doi.org/10.2741/2296.

57. Mavrogiannis, L.A., Antonopoulou, I., Baxová, A., Kutílek, S., Kim, C.A., Sugayama, S.M., Salamanca, A., Wall, S.A., Morriss-Kay, G.M., and Wilkie, A.O. (2001). Haploinsufficiency of the human homeobox gene ALX4 causes skull ossification defects. Nat. Genet. *27*, 17–18. https://doi.org/10.1038/83703.

58. Farmer, D.T., Mlcochova, H., Zhou, Y., Koelling, N., Wang, G., Ashley, N., Bugacov, H., Chen, H.-J., Parvez, R., Tseng, K.-C., et al. (2021). The developing mouse coronal suture at single-cell resolution. Nat. Commun. *12*, 4797. https://doi.org/10.1038/s41467-021-24917-9.

59. Zhang, J., Zhang, W., Dai, J., Wang, X., and Shen, S.G. (2019). Overexpression of Dlx2 enhances osteogenic differentiation of BMSCs and MC3T3-E1 cells via direct upregulation of Osteocalcin and Alp. Int. J. Oral Sci. *11*, 12. https://doi.org/10.1038/s41368-019-0046-1.

60. Shang, N., Bhullar, K.S., and Wu, J. (2020). Ovotransferrin Exhibits Osteogenic Activity Partially via Low-Density Lipoprotein Receptor-Related Protein 1 (LRP1) Activation in MC3T3-E1 Cells. J. Agric. Food Chem. *68*, 9427–9435. https://doi.org/10.1021/acs.jafc.0c04064.

61. Chan, W.C.W., Tan, Z., To, M.K.T., and Chan, D. (2021). Regulation and Role of Transcription Factors in Osteogenesis. Int. J. Mol. Sci. *22*, 5445. https://doi.org/10.3390/ijms22115445.

62. Marie, P.J., Haÿ, E., and Saidak, Z. (2014). Integrin and cadherin signaling in bone: role and potential therapeutic targets. Trends Endocrinol. Metab. *25*, 567–575. https://doi.org/10.1016/j.tem.2014.06.009.

63. Gu, J., Lu, Y., Li, F., Qiao, L., Wang, Q., Li, N., Borgia, J.A., Deng, Y., Lei, G., and Zheng, Q. (2014). Identification and characterization of the novel Col10a1 regulatory mechanism during chondrocyte hypertrophic differentiation. Cell Death Dis. *5*, e1469. https://doi.org/10.1038/cddis.2014.444.

64. Ji, Q., Zheng, Y., Zhang, G., Hu, Y., Fan, X., Hou, Y., Wen, L., Li, L., Xu, Y., Wang, Y., and Tang, F. (2019). Single-cell RNA-seq analysis reveals the progression of human osteoarthritis. Ann. Rheum. Dis. *78*, 100–110. https://doi.org/10.1136/annrheumdis-2017-212863.

65. Yang, G., Zhu, L., Hou, N., Lan, Y., Wu, X.-M., Zhou, B., Teng, Y., and Yang, X. (2014). Osteogenic fate of hypertrophic chondrocytes. Cell Res. *24*, 1266–1269. https://doi.org/10.1038/cr.2014.111.

66. Kalna, V., Yang, Y., Peghaire, C.R., Frudd, K., Hannah, R., Shah, A.V., Osuna Almagro, L., Boyle, J.J., Göttgens, B., Ferrer, J., et al. (2019). The Transcription Factor ERG Regulates Super-Enhancers Associated With an Endothelial-Specific Gene Expression Program. Circ. Res. *124*, 1337–1349. https://doi.org/10.1161/CIRCRESAHA.118.313788.

67. Wuelling, M., Schneider, S., Schröther, V.A., Waterkamp, C., Hoffmann, D., and Vortkamp, A. (2020). Wnt5a is a transcriptional target of Gli3 and Trps1 at the onset of chondrocyte hypertrophy. Dev. Biol. *457*, 104–118. https://doi.org/10.1016/j.ydbio.2019.09.012.

68. Veistinen, L.K., Mustonen, T., Hasan, M.R., Takatalo, M., Kobayashi, Y., Kesper, D.A., Vortkamp, A., and Rice, D.P. (2017). Regulation of Calvarial Osteogenesis by Concomitant De-repression of GLI3 and Activation of IHH Targets. Front. Physiol. *8*, 1036. https://doi.org/10.3389/fphys.2017.01036.

69. Hayashi, M., Nakashima, T., Taniguchi, M., Kodama, T., Kumanogoh, A., and Takayanagi, H. (2012). Osteoprotection by semaphorin 3A. Nature *485*, 69–74. https://doi.org/10.1038/nature11000.

70. Chan, C.K.F., Gulati, G.S., Sinha, R., Tompkins, J.V., Lopez, M., Carter, A.C., Ransom, R.C., Reinisch, A., Wearda, T., Murphy, M., et al. (2018). Identification of the Human Skeletal Stem Cell. Cell *175*, 43–56.e21. https://doi.org/10.1016/j.cell.2018.07.029.

71. Provot, S., Zinyk, D., Gunes, Y., Kathri, R., Le, Q., Kronenberg, H.M., Johnson, R.S., Longaker, M.T., Giaccia, A.J., and Schipani, E. (2007). Hif-1alpha regulates differentiation of limb bud mesenchyme and joint development. J. Cell Biol. *177*, 451–464. https://doi.org/10.1083/jcb.200612023.

72. Schmid, R., Meyer, K., Spang, R., Schittek, B., and Bosserhoff, A.K. (2013). YBX1 is a modulator of MIA/CD-RAP-dependent chondrogenesis. PLoS One *8*, e82166. https://doi.org/10.1371/journal.pone.0082166.

73. Pilquil, C., Alvandi, Z., and Opas, M. (2020). Calreticulin regulates a switch between osteoblast and chondrocyte lineages derived from murine embryonic stem cells. J. Biol. Chem. *295*, 6861–6875. https://doi.org/10.1074/jbc.RA119.011029.

74. Bunis, D.G., Andrews, J., Fragiadakis, G.K., Burt, T.D., and Sirota, M. (2021). dittoSeq: Universal User-Friendly Single-Cell and Bulk RNA Sequencing Visualization Toolkit. Bioinformatics *36*, 5535–5536. https://doi.org/10.1093/bioinformatics/btaa1011.

75. Stoeckius, M., Zheng, S., Houck-Loomis, B., Hao, S., Yeung, B.Z., Mauck, W.M., Smibert, P., and Satija, R. (2018). Cell Hashing with barcoded antibodies enables multiplexing and doublet detection for single cell genomics. Genome Biol. *19*, 224. https://doi.org/10.1186/s13059-018-1603-1.

76. Reimand, J., Kull, M., Peterson, H., Hansen, J., and Vilo, J. (2007). g:Profiler–a web-based toolset for functional profiling of gene lists from large-scale experiments. Nucleic Acids Res. *35*, W193–W200. https://doi.org/10.1093/nar/gkm226.

77. Tirosh, I., Izar, B., Prakadan, S.M., Wadsworth, M.H., Treacy, D., Trombetta, J.J., Rotem, A., Rodman, C., Lian, C., Murphy, G., et al. (2016). Dissecting the multicellular ecosystem of metastatic melanoma by single-cell RNA-seq. Science *352*, 189–196. https://doi.org/10.1126/science.aad0501.

STAR★METHODS

KEY RESOURCES TABLE

REAGENT or RESOURCE	SOURCE	IDENTIFIER
Antibodies		
Rabbit polyclonal to Collagen I antibody	Abcam	Cat#ab34710; RRID:AB_731684
Mouse monoclonal $IgG_{2b}\kappa$ COL2A1 antibody	Santa Cruz	Cat#sc-52658; RRID:AB_2082344
Sheep polyclonal to Von Willebrand Factor antibody	Abcam	Cat#ab11713; RRID:AB_298501
Goat polyclonal to alpha smooth muscle Actin antibody	Abcam	Cat#ab21027; RRID:AB_1951138
Rabbit monoclonal to YB1 antibody	Abcam	Cat#ab76149; RRID:AB_2219276
Rabbit monoclonal to HIF-1 alpha antibody	Abcam	Cat#ab51608; RRID:AB_880418
Rabbit monoclonal to Fos B antibody	Abcam	Cat#ab184938; RRID:AB_2721123
Mouse monoclonal IgG_1 NF-1 antibody	Santa Cruz	Cat#sc74445; RRID:AB_2153046
Mouse monoclonal $IgG_1\kappa$ Erg-1/2/3 antibody	Santa Cruz	Cat#sc376293; RRID:AB_10989086
Rabbit monoclonal to Semaphorin 3A antibody	Abcam	Cat#ab199475
Goat Polyclonal IgG to GLI-3 antibody	R&D SYSTEMS	Cat#AF3690-SP
Mouse monoclonal $IgG_1\kappa$ Mig-6 antibody	Santa Cruz	Cat#sc137154; RRID:AB_2101524
Goat polyclonal to Asporin antibody	Abcam	Cat#ab31303; RRID:AB_2060301
Rabbit monoclonal to IGF1 antibody	Abcam	Cat#ab133542
Mouse monoclonal to CD63 antibody	Abcam	Cat#ab193349
Mouse monoclonal IgG_{2b}LRP1 antibody	Santa Cruz	Cat#sc57351; RRID:AB_784362
Mouse monoclonal $IgG_{2b}\kappa$ Calregulin antibody	Santa Cruz	Cat#sc373863; RRID:AB_10915425
Mouse monoclonal $IgG_{2b}\kappa$ ATF4 antibody	Santa Cruz	Cat#sc390063; RRID:AB_2810998
Goat Anti-Mouse IgM (Alexa Fluor® 555)	Bioss	Cat#bs-0368G-AF555
Donkey Anti-Mouse IgG H&L (Alexa Fluor® 488)	Abcam	Cat#ab150105; RRID:AB_2732856
Goat Anti-Rabbit IgG H&L (FITC)	Bioss	Cat#bs-0295G-FITC; RRID:AB_10894349
Donkey Anti-Rabbit IgG H&L (Alexa Fluor® 488)	Abcam	Cat#ab150073; RRID:AB_2636877
Donkey Anti-Mouse IgG H&L (Alexa Fluor® 555)	Abcam	Cat#ab150110; RRID:AB_2783637
Goat Anti-Rabbit IgG H&L (Alexa Fluor® 555)	Abcam	Cat#ab150078; RRID:AB_2722519
Donkey Anti-Sheep IgG H&L (Alexa Fluor® 488)	Abcam	Cat#ab150177; RRID:AB_2801320
Donkey Anti-Goat IgG H&L (Alexa Fluor® 488) preadsorbed	Abcam	Cat#ab150133; RRID:AB_2832252
Biological samples		
4 Human fetal samples of age post conception week 15, 19, 22, and 25 (Table S6)	This paper	N/A
14 Human fetal samples of age post conception week 12 to 32 (Table S6)	This paper	N/A
Human Cord blood mesenchymal stem cells	iCell Bioscience Inc	Cat#HUM-iCell-e011
Human Placental Mesenchymal Stem Cells	iCell Bioscience Inc	Cat#HUM-iCell-e004

(*Continued on next page*)

Continued

REAGENT or RESOURCE	SOURCE	IDENTIFIER
Critical commercial assays		
Chromium Next GEM Single Cell 3′ GEM kit v3.1	10× Genomics	Cat#PN-1000123
Non - Serum Culture System Of Primary Mesenchymal Stem Cells Of ICell	iCell Bioscience Inc	Cat#PriMed-iCell-012-SF
Mesenchymal stem cell chondrogenic differentiation kit	iCell Bioscience Inc	Cat#iCell-MSCYD-003
Mesenchymal stem cell osteogenic differentiation kit	iCell Bioscience Inc	Cat#iCEll-MSCYD-002
Toluidine Blue O	Sigma Aldrich	Cat#T3260
Cartilage staining solution (Alcian blue method, pH2.5)	LEAGENE	Cat#DB0060
1-Step™ NBT/BCIP Substrate Solution	Thermo Scientific	Cat#34042
Steadypure Quick RNA Extraction Kit	Accurate biology	Cat#AG21023
Sunview® III Reverse Transcriptase kit	SUNVIEW	Cat#RT008
Sunview® SYBR qPCR SuperMix Plus	SUNVIEW	Cat#QE010-02
Deposited data		
The original matrix datasets derived from the raw single-cell RNA-seq data in this study.	Mendeley Data	https://doi.org/10.17632/3c6sy3tyyv.1
The code for single-cell RNA-seq analysis in this study.	Zenodo	https://doi.org/10.5281/zenodo.8021217
Software and algorithms		
R	R core team	version 4.1.3
R studio	Posit Community	version 2022.02.1 Build 461
Seurat	Satija Lab and Collaborators[22]	version 4.1.1; RRID:SCR_016341
GSVA	Hänzelmann, S.[29]	version 1.42.0; RRID:SCR_021058
monocle	Trapnell, C.[32,33]	version 2.22.0; RRID:SCR_016339
SCENIC	Van de Sande and Aibar, S.[30,31]	version 1.3.1; RRID:SCR_017247
CellChat	Jin, S.[41]	version 1.4.0; RRID:SCR_021946
dittoSeq	Bunis, D.G.[74]	version 1.6.0
python	The Python Software Foundation	version 3.7.12; RRID:SCR_008394
pySCENIC	Van de Sande and Aibar, S.[30,31]	version 0.11.2
Design and Analysis Software v1.5.2, QuantStudio 3 and 5 systems	applied biosystems	version 1.5.1
cellSens Imaging Software	OLYMPUS	version 3.2; RRID:SCR_014551
Image-Pro Plus	Media Cybernetics	version 6.0; RRID:SCR_016879
GraphPad Prism	GraphPad Software	version 8; RRID:SCR_002798

RESOURCE AVAILABILITY

Lead contact

Further information and requests for resources and reagents should be directed to and will be fulfilled by the lead contact, Liang Zhao (lzhaonf@126.com and lzhaogroup@163.com).

Materials availability

This study did not generate new unique reagents.

Data and code availability

- Local law prohibits depositing raw RNA sequencing datasets derived from human samples outside of the country of origin. Prior to publication, the authors officially requested that the raw single-cell RNA-seq datasets reported in this paper be made publicly accessible. To request access, contact National Genomics Data Center until the date approved. In addition, the original matrix datasets derived from the raw single-cell RNA-seq data in this study have been deposited at mendeley data and are publicly available as of the date of publication (Mendeley Data: https://doi.org/10.17632/3c6sy3tyyv.1). The DOI is listed in the key resources table.
- All original code will be deposited at Zenodo and is publicly available as of the date of publication (Zenodo: https://doi.org/10.5281/zenodo.8021217). DOIs are listed in the key resources table.
- Any additional information required to reanalyze the data reported in this paper is available from the lead contact upon request.

EXPERIMENTAL MODEL AND STUDY PARTICIPANT DETAILS

Human tissue

Human distal femoral epiphysis tissue was obtained in the obstetrics of Nanfang Hospital and its Taihe Branch, from spontaneous abortions (12-32 weeks post-conception) and with an ethical permit given by the Nanfang Hospital Ethical Medical Committee (ref. NFEC-2020-166). Samples with chromosomal defects found by regular obstetric inspection have been excluded. A total of 22 samples were obtained for this study, 4 of which were subjected to scRNA-seq (PCW15, male; PCW19, male; PCW22, female; PCW25, male, Table S6), 14 of which were subjected to paraffin sections(PCW12∼32, male or female, Table S6), 4 of which failed to yield enough vital cells and were discarded. The conditions of consent were voluntary, anonymous, and with the awareness that the donations will be used for research.

METHOD DETAILS

scRNA-SEQ samples preparation

The human fetal distal femur was collected and stored in complete culture medium (αMEM, Gibco; 10% fetal bovine serum[FBS], Sunview; 1% Penicillin/streptomycin, gibco) during transshipment (4°C, less than 30min). The epiphyseal tissue used for this study refers to the expanded cartilaginous area at the distal end of the femur. The anatomical landmark was the expansion point from the diaphysis to the distal end. Femurs were cut off along this anatomical landmark and the ossified tissue (from the primary ossification center) across the sectional plane was removed. The soft tissue attached to the epiphysis surface was also removed. Tissue was then cut into pieces 1-2mm in size and placed in a tissue culture flask for two-step digestion. First, tissue was digested in αMEM supplemented with 7U/ml pronase (Roshe, 37°C in a shaking box under 60rpm for 30min). The digestion solution from this step was discarded. Next, complete culture medium supplemented with 0.2% collagenase I(Sigma) and collagenase II(Sigma) was used for the second digestion(37°C in a shaking box under 60rpm for ∼120min, depending on observation). When digestion was completed, the isolated cells floating in the digestion solution could be observed under a microscope. Finally, collected cells were stored on ice with PBS containing 3% FBS and sent to a qualified facility offering scRNA-seq service(Yuanxin Biotechnology) within 1hr. Samples with a cell viability rate greater than 85% and yielded cell numbers greater than 50,000 were immediately prepared for single-cell library preparation.

scRNA-SEQ

This section was performed by Yuanxin Biotechnology in a standard procedure. Approximately 18,000 cells per sample were partitioned into nanoliter-scale Gel Beads-in-emulsion (GEMs), followed by post-GEM-RT cleanup, cDNA amplification, and 3′ gene expression library construction under the instruction of a commercial kit (Chromium Next GEM Single Cell 3′ GEM kit v3.1, 10X Genomic). Subsequent analysis pipelines that process sequencing data to align reads, filter, barcode count, UMI count, and generate feature-barcode matrices were performed using the software Cell Ranger (version 6.1.2) under its instruction.

scRNA-SEQ data analysis

Feature-barcode matrices of each sample generated by Cell Ranger were used for scRNA-SER data analysis.

The quality control(QC) of each sample was carried out under the following basic rules in order. (1) The matrix was used to construct the primary Seurat object with eliminating genes detected in <1 cell and discarding cells with features count <250 by using an R package Seurat[22](version 4.1.1). (2) Cells with mitochondrial percent >20%, ribosomal percent <10%, hemoglobin percent >0.05%, and platelet percent >0.2% were discarded. (3) Mitochondrial and MALAT1 genes were eliminated as these genes were thought to be judged as mainly technical. (4) Doublets identified by R package DoubletFinder[75] (version 2.0) were discarded. (5) Outlier cells with RNA count and feature count outside the range of $\pm$ 3 $\times$ median absolute deviation (MAD) were discarded. After QC, samples from PCW15 (with 30,036 features across 10,109 cells), PCW19 (with 32,754 features across 10,620 cells), PCW22 (with 33,997 features across 5,656 cells), and PCW25 (with 31320 features across 8,613 cells) were preserved for downstream analysis. Correlations between nFeature_RNA or percent_mito and nCount_RNA were visualized by scatter plots.

The filtered data were then integrated using Seurat. Raw counts were normalized with the SCTransform function with multiple regression variables, including percent_mito, percent_ribo, S.Score, and G2M.Score, nFeature_RNA, and nCount_RNA. 3,000 variable features were used in the downstream integration procedure. Next, cross-dataset pairs of cells in a matched biological state were identified and technical differences between samples were corrected using a combination of the SelectIntegrationFeatures, PrepSCTIntegration, and FindIntegrationAnchors functions. Finally, integrated data for the comparative scRNA-seq analysis across 4 samples were generated by the IntegrateData function.

Cells were then clustered using K-nearest neighbor (KNN) graphs and the Louvain algorithm using the first 50 dimensions from principal component analysis (PCA). Clustered cells were visualized by UMAP embedding using modified settings in Seurat. Cell proportions were visualized by bar graphs using the R package dittoseq[74] (version 1.6.0). Cluster markers were identified as features detected in $\geq$10% of either cluster, with logfc.threshold >0.25 and adjusted p-value<0.01 compared to the others using the FindAllMarkers function in Seurat. Selected top markers were ordered by avg_log2FC and visualized by heatmaps. Major cell types were identified using canonical gene markers visualized by UMAPs, dot plots, and violin plots.

Genes for GO enrichment analysis were acquired from cluster markers after filtering ribosome genes. The top 50 genes ordered by the incrementally adjusted p-value of each subtype were subjected to an online GO enrichment analysis platform named g:GOSt (https://biit.cs.ut.ee/gprofiler/gost).[76] Enriched GOBP terms in each subtype were considered as a reference of cell functions. Annotations of the cells were based on the canonical gene markers expression, cluster markers, and involved GOBPs.

Cells were reclassified into 9 populations according to the gene signatures and GOBPs to highlight the difference in functions. Genes annotated to GO:0001958 (endochondral ossification) and GO:0051216 (cartilage development) were acquired from the MGI database (http://www.informatics.jax.org/vocab/gene_ontology). Average expression levels of these feature sets in each population were calculated by the AddModuleScore function[77] and visualized by box plots using dittoSeq.

pySCENIC(version 0.11.2), the python implementation of the SCENIC pipeline,[30,31] was used to analyze GRNs. Normalized counts of the integrated cells were subjected to this analysis. GRNBoost was the algorithm used to build the GRN with default settings. AUC scores of the potential direct-biding targets (regulons) were calculated for analyzing the network activity in each individual cell. Average regulons activity across 9 populations were calculated, scaled, and visualized by a heatmap. Furthermore, the AUC matrix was added to the integrated Seurat object as an independent assay using the CreateAssayObject function in Seurat.

GSVA was performed on a random subset of 5,000 cells from the integrated data using the R package GSVA (version 1.42.0).[29] Ontology gene sets (C5, all, version 7.5.1) reference was obtained from Human MSigDB (http://www.gsea-msigdb.org/gsea/msigdb/collections.jsp). A matrix containing GSVA enrichment scores of each individual cell was generated by the gsva function with kcdf = Poisson as the input expression values were counts. The matrix was added to the subset Seurat object as an independent assay using the CreateAssayObject function in Seurat. Thereafter, differentially enriched terms with logfc.threshold $\geq$0.1 and adjusted p-value <0.01 across 24 subtypes were calculated using the FindAllMarkers function in Seurat. The top 10 GOBP enriched terms ordered by avg_log2FC across 24 subtypes were visualized by heatmap.

Three subset strategies were performed to construct datasets for trajectory analysis in this study independently. Within the Cartilage development population, 500 cells per sample were subset randomly from the integrated data. Within the Ossification development population, 300 cells per sample were subset randomly from the integrated data. 120 cells from each population per sample across the Cartilage development, Ossification development, and Intermediate cell populations were subset randomly from the integrated data. Thus, the cells of each population from each sample were equal, aiming to reduce the bias induced by different cell numbers. These datasets were analyzed independently using the R package Monocle2. Ribosome and hemoglobin genes were filtered out before analysis. Differential expression tests were performed by the differentialGeneTest function with key settings including fullModelFormulaStr = "~Samples" and reducedModelFormulaStr = "~nCount_RNA+nFeature_RNA+percent_ribo+percent_mito" in Monocle2. Differential expression genes with qval <0.01 were used for downstream dimension reduction based on identifying the program of gene expression changes via the algorithm DDRTree. Thereafter, trajectories were constructed, and cell states were defined using the orderCells function with default settings in Monocle2. Genes with branch-dependent expression were analyzed using the BEAM function with default settings in Monocle2. The top 100 or 200 genes ordered by decreasing q-value were visualized by heatmap and clustered hierarchically. The expression levels of selected genes over pseudotime were visualized to show the trends across different trajectories. Genes of each subtype were subjected to GO enrichment analysis with visualization of selected GOBP enriched terms with the lowest adjusted p-value. Cell state information was used to re-ident the cells in the subset Seurat object. Thereafter, the regulons with different activities(AUC scores) were calculated by the FindAll Markers function. The top 5 regulons with the highest log2fold changes of each state were visualized by heatmap. The transcriptome factor from each regulon was visualized by box plots across the four samples. The transcriptome factors with detectable expression levels were used to screen out those with matched trends between samples' age and Monocle's pseudotime.

The cell-cell communication analysis was performed on each sample independently using the R package CellChat (version 1.4.0).[41] Here, the integrated data (Seurat object) was split by sample identities. 3,000 cells per sample were subset randomly for downstream cell-cell communication analysis. The reference database of three types of cell-cell communication including secreted signaling, ECM-receptor signaling, and cell-cell contact signaling was used to infer the intercellular interactions through the pipeline with default settings in CellChat. The numbers and strength of inferred interactions in each sample were visualized by bar plots. Scatter plots were used to visualize the incoming and outgoing interaction strength of each across the 24 subtypes. Circle plots were used to visualize the interaction strengths among the 9 populations. Next, two samples at adjacent time points were merged and compared. The information flow for each signaling pathway is defined by the sum of communication probability among all pairs of cell groups in the inferred network. The information flow between the compared samples was visualized by bar graphs. Differential expression analysis of genes between 2 samples was performed using the identifyOverExpressedGenes function with settings thresh.pc = 0.05, thresh.fc = 0.1, and thresh.p = 0.05 in CellChat. Wordcloud was generated to visualize the enriched ligands in one sample compared to another. Ligand and receptor expressions involved in selected signalings, such as *NOTCH* and *FGF*, were visualized by stack violin plots. Chord diagrams were used to visualize interactions among 9 populations via selected ligand-receptor pairs. The heatmap exhibiting the expressions of targets of *NOTCH* signaling was generated via the DoHeatmap function of the Seurat package. The dot plot exhibiting the expressions of ligands, receptors, and targets of *NOTCH* signaling as well as genes correlating to endochondral ossification of cells in State 4 of PCW19 and PCW22 during ossification development was generated via the DotPlot function of the Seurat package. Significant interactions (L-R pairs) from some cell subtypes/populations to others were visualized by bubble plots.

Cell culture

The primary human umbilical cord blood mesenchymal stem cells (UBMSCs, cat#HUM-iCell-e011) and placental mesenchymal stem cells (PMSCs, cat#HUM-iCell-e004) were purchased from iCell bioscience company and delivered in a 25 cm^2 culture flask with complete culture media. Cells were cultured under 37°C and 5% CO2 in an incubator with complete culture media(iCell, cat#PriMed-iCell-012-SF), trypsinized when reached 80% confluence, and passaged at 5000 cells/cm^2 for further cell number expansion before re-seeding for differentiation experiment.

Chondrogenesis differentiation

MSCs were trypsinized when reached 80% confluence and re-seeded at 1×10^5/10μL each well in 24-well-plates for micromass culture. After the cells were left standing in the incubator for 2 hours, the complete

culture medium was added. Cells were cultured overnight and then divided into control group with control media (without chondrogenesis compounds) and chondrogenesis group with chondrogenesis media (iCell, cat#iCEll-MSCYD-003) (with TGF-β1, ascorbic acid, ITS, and dexamethasone). Three biological repeats were set up. Induction media was changed every other day. RNA was collected on Day 0, 1, 5 ,14, 21 and toluidine blue and Alcian blue staining were performed on Day 14.

Osteogenesis differentiation

MSCs were trypsinized when reached 80% confluence and re-seeded at $1.5\times10^4/cm^2$ in 24-well-plates prior coated with 1% gelatin solution. Cells were cultured overnight with complete culture media and then divided into control group with control media (without osteogenesis compounds) and osteogenesis group with osteoogenesis media (iCell, cat#iCEll-MSCYD-002) (with ascorbic acid, β-lycerophosphate, and dexamethasone). Three biological repeats were set up. Induction media was changed every other day. RNA was collected on Day 0, 3,5, 7 and ALP staining were performed on Day 7.

Cell staining and capture

MSCs under chondrogenesis induction on Day 14 were stained with toluidine blue and Alcian blue respectively. For toluidine blue staining, cells were fixed by treating with 4% paraformaldehyde (PFA) for 10 min, washed with DPBS for 3 time and stained with 0.1% toluidine blue staining buffer for 15 min. The 0.1% toluidine blue staining buffer is a mixture of toluidine blue (Sigma, cat#T3260-5G, 0.5g), urea (Fisher Scientific, cat#BP169-500, 1g), ethonal (150mL), and water (350mL). For Alcian blue staining, fixed and washed cells were stained with a commercial Alcian blue staining buffer (LEAGENE, cat#DB0060) according to the instruction. For ALP staining, fixed and washed cells were stained with a commercial ALP staining buffer (Thermo Scientific, cat#34042) according to the instruction. After staining cells were washed with water for 3 times and dried at room temperature. The cells stained with toluidine blue and Alcian blue were scanned by an EPSON scanner. Microscopic pictures were captured via a combination of OLYMPUS DP80 camera, OLYMPUS IX73 microscope, and imaging software cellSens (version 3.2).

RNA extraction, purification and reverse transcription

RNAs of MSCs during differentiation induction were extracted and purified using a commercial RNA extraction kit (Accurate Biology, cat#AG21023) according to its instruction. The concentration of RNAs were measured by Thermo Scientific Nanodrop ONE^C. The Reverse transcription of RNAs were accomplished by using commercial kits (SUNVIEW, cat#RT008) and PCR machine (Biometra TADVANCED, sn.3324551) (25°C for 10min, 55°C for 30min, 85°C for 5min, and 4°C for long). The synthesized cDNAs were diluted to 2.5 ng/μL according to the RNAs concentration. cDNAs were used for quantitative Real-time PCR measurements.

Quantitative real-time PCR (qPCR)

The master mix for qPCR was generated using cDNA, primers (Table S7) and a commercial kit (SUNVIEW, cat#QE010-02). Three technical repeats were set for each sample. Samples tested for the same gene were all on the same 384-qPCR-plate (applied biosystem, cat#4309849). qPCR was accomplished using an applied biosystem Quant Studio 5.

Paraffin sections and IF staining

The human epiphysis tissues for paraffin sections were fixed in 4% paraformaldehyde (PFA) at 4°C overnight. After cleaning, dehydration, clearing, and paraffin impregnation, the samples were embedded into paraffin blocks. Sagittal sections with a thickness of 4 μm were collected for IF staining. Sections were stained with primary antibodies (Table S8) overnight, and probed with matched secondary antibodies (Table S8). A mounting medium supplement with DAPI (Abcam ab104139) was used to stain the nucleic acid. Olympus BX63 Microscope, light source model U-HGLGPS, OLYMPUS DP80 cameras, and imaging software cellSens (version 3.2) were used to capture the pictures of stained sections.

QUANTIFICATION AND STATISTICAL ANALYSIS

The positive signals of IF staining were quantified using Image-Pro Plus (version 6.0) in a blinded fashion. Positive IOD and area were measured to calculate IOD/Area for each measured object from each section. The intraluminal area of cartilage canals was excluded for quantification avoiding the bias brought by the fluorescent signals produced by red blood cells. Scatter dot plots and box plots were used to visualize the

quantification results with error bars representing mean ± SD. Bar plots were used to visualize the qPCR results with error bars representing mean ± SEM. Statistical tests and the number of samples used are listed in the figure legends. Group comparisons were performed using a t-test when two groups were compared. One-way ANOVA was used when three or more groups were compared. Statistical analyses were performed by using the GraphPad Prism software or R. All p-values were denoted as ns for $p \geq 0.05$, *for $p < 0.05$, **for $p < 0.01$, ***for $p < 0.001$, and ****for $p < 0.0001$. For all statistical analyses and unless otherwise specified, p-values < 0.05 were deemed significant.